QUARTERLY JOURNAL OF THE ROYAL METEOROLOGICAL SOCIETY
Q. J. R. Meteorol. Soc. (2009)
Published online in Wiley InterScience
(www.interscience.wiley.com) DOI: 10.1002/qj.416

Intercomparison of model simulations of mixed-phase clouds observed during the ARM Mixed-Phase Arctic Cloud Experiment. I: Single-layer cloud

Stephen A. Klein,[a]* Renata B. McCoy,[a] Hugh Morrison,[b] Andrew S. Ackerman,[c],† Alexander Avramov,[d] Gijs de Boer,[e] Mingxuan Chen,[f] Jason N. S. Cole,[g] Anthony D. Del Genio,[c],† Michael Falk,[h] Michael J. Foster,[i] Ann Fridlind,[c],† Jean-Christophe Golaz,[j] Tempei Hashino,[e] Jerry Y. Harrington,[d] Corinna Hoose,[k] Marat F. Khairoutdinov,[l] Vincent E. Larson,[h] Xiaohong Liu,[m] Yali Luo,[n] Greg M. McFarquhar,[o] Surabi Menon,[p] Roel A. J. Neggers,[q] Sungsu Park,[r] Michael R. Poellot,[s] Jerome M. Schmidt,[t],† Igor Sednev,[p] Ben J. Shipway,[u],‡ Matthew D. Shupe,[v] Douglas A. Spangenberg,[w] Yogesh C. Sud,[x],† David D. Turner,[e] Dana E. Veron,[y] Knut von Salzen,[z] Gregory K. Walker,[x] Zhien Wang,[aa] Audrey B. Wolf,[c] Shaocheng Xie,[a] Kuan-Man Xu,[bb],† Fanglin Yang[cc] and Gong Zhang[o]

[a]*Lawrence Livermore National Laboratory, Livermore, California, USA;* [b]*National Center for Atmospheric Research, Boulder, Colorado, USA;* [c]*NASA Goddard Institute for Space Studies, New York, NY, USA;* [d]*The Pennsylvania State University, University Park, PA, USA;* [e]*University of Wisconsin – Madison, Madison, WI, USA;* [f]*Colorado State University, Fort Collins, CO, USA;* [g]*University of British Columbia, Vancouver, BC, Canada;* [h]*University of Wisconsin – Milwaukee, Milwaukee, WI, USA;* [i]*Rutgers University, New Brunswick, New Jersey, USA;* [j]*NOAA Geophysical Fluid Dynamics Laboratory, Princeton, New Jersey, USA;* [k]*ETH Zurich, Institute for Atmospheric and Climate Science, Zurich, Switzerland;* [l]*State University of New York at Stony Brook, Stony Brook, NY, USA;* [m]*Pacific Northwest National Laboratory, Richland, Washington, USA;* [n]*State Key Laboratory of Severe Weather, Chinese Academy of Meteorological Sciences, Beijing, China;* [o]*University of Illinois, Urbana, IL, USA;* [p]*Lawrence Berkeley National Laboratory, Berkeley, California, USA;* [q]*KNMI, Utrecht, Netherlands;* [r]*University of Washington, Seattle, WA, USA;* [s]*University of North Dakota, Grand Forks, ND, USA;* [t]*Navy Research Laboratory, Monterey, California, USA;* [u]*Met Office, Exeter, United Kingdom;* [v]*Cooperative Institute for Research in Environmental Sciences, University of Colorado/NOAA, Boulder, CO, USA;* [w]*Science Systems and Applications, Inc., Hampton, Virginia, USA;* [x]*NASA Goddard Space Flight Center, Greenbelt, Maryland, USA;* [y]*University of Delaware, Newark, DE, USA;* [z]*Canadian Center for Climate, Vancouver, British Columbia, Canada;* [aa]*University of Wyoming, Laramie, WY, USA;* [bb]*NASA Langley Research Center, Hampton, Virginia, USA;* [cc]*National Centers for Environmental Prediction, Camp Springs, Maryland, USA*

ABSTRACT: Results are presented from an intercomparison of single-column and cloud-resolving model simulations of a cold-air outbreak mixed-phase stratocumulus cloud observed during the Atmospheric Radiation Measurement (ARM) programme's Mixed-Phase Arctic Cloud Experiment. The observed cloud occurred in a well-mixed boundary layer with a cloud-top temperature of −15°C. The average liquid water path of around 160 g m^{-2} was about two-thirds of the adiabatic value and far greater than the average mass of ice which when integrated from the surface to cloud top was around 15 g m^{-2}.

Simulations of 17 single-column models (SCMs) and 9 cloud-resolving models (CRMs) are compared. While the simulated ice water path is generally consistent with observed values, the median SCM and CRM liquid water path is a factor-of-three smaller than observed. Results from a sensitivity study in which models removed ice microphysics suggest that in many models the interaction between liquid and ice-phase microphysics is responsible for the large model underestimate of liquid water path.

Despite this underestimate, the simulated liquid and ice water paths of several models are consistent with observed values. Furthermore, models with more sophisticated microphysics simulate liquid and ice water paths that are in better agreement with the observed values, although considerable scatter exists. Although no single factor guarantees a good simulation, these results emphasize the need for improvement in the model representation of mixed-phase microphysics.

KEY WORDS mixed-phase cloud; Arctic clouds; single-column models; cloud-resolving models

Received 5 March 2008; Revised 23 February 2009; Accepted 2 March 2009

*Correspondence to: Stephen A. Klein, PCMDI, Lawrence Livermore National Laboratory, Livermore, California, 94551, USA. E-mail: klein21@llnl.gov

†The contributions of Andrew S. Ackerman, Anthony D. Del Genio, Ann Fridlind, Jerome M. Schmidt, Yogesh C. Sud, and Kuan-Man Xu to this article were prepared as part of their official duties as United States Federal Government employees.

‡The contribution of Ben J. Shipway was written in the course of his employment at the Met Office, UK and is published with the permission of the Controller of HMSO and the Queen's Printer for Scotland.

1. Introduction

The treatment of clouds continues to be a highly challenging aspect of climate and weather modelling. Parametrization of Arctic clouds has been especially difficult, given the paucity of observations in the region (Curry *et al.*, 1996). However, several field programmes in recent years have begun to address this deficiency, including the 1994 Beaufort and Arctic Storms Experiment (Curry *et al.*, 1997), the 1997–1998 Surface Heat Budget of the Arctic Ocean Experiment (SHEBA: Uttal *et al.*, 2002), the 1998 First International Satellite Cloud Climatology Project Regional Experiment – Arctic Clouds Experiment (Curry *et al.*, 2000), and the ongoing Atmospheric Radiation Measurement (ARM) programme site operating near Barrow, Alaska (Ackerman and Stokes, 2003).

A major finding of these experiments was the observed frequency and persistence of supercooled liquid water and mixed-phase stratiform clouds throughout the year (Curry *et al.*, 2000; Pinto *et al.*, 2001; Intrieri *et al.*, 2002; Korolev *et al.*, 2003; Shupe and Intrieri, 2004). In contrast to midlatitude cloud systems, there is little temperature dependence for the amount of liquid versus ice in Arctic mixed-phase clouds (Curry *et al.*, 2000; Korolev *et al.*, 2003; McFarquhar and Cober, 2004; Turner, 2005). These clouds may contain one or more thin liquid layers embedded within a deep cloud that extends from near the surface into the middle and upper troposphere (Hobbs and Rangno, 1998; Pinto, 1998; Shupe *et al.*, 2006). Ice crystals falling from liquid layers may reach the ground in the form of light snow or snow showers. During SHEBA, slightly more than half of mixed-phase clouds consisted of a single low-level liquid layer, while the rest consisted of multiple liquid layers in a deep cloud ice layer (Shupe *et al.*, 2006).

The frequent occurrence of mixed-phase clouds has important implications for the cloud radiative forcing at the surface, since mixed-phase clouds tend to be optically thicker than ice-only clouds (Sun and Shine, 1994; Shupe and Intrieri, 2004; Turner, 2005; Zuidema *et al.*, 2005). The presence of mixed-phase as compared to ice-only clouds may also significantly impact the structure of the boundary layer and large-scale dynamics through the influence of cloud-top radiative cooling (Morrison and Pinto, 2006).

Climate and weather models tend to have difficulty predicting the observed frequency and persistence of Arctic mixed-phase clouds, leading to biases in surface radiative fluxes (Curry *et al.*, 2000; Girard and Curry, 2001; Morrison *et al.*, 2003, 2005b; Inoue *et al.*, 2006; Morrison and Pinto, 2006; Prenni *et al.*, 2007; Sandvik *et al.*, 2007). These models tend to have difficulty simulating midlatitude mixed-phase clouds as well (Illingworth *et al.*, 2007). Studies have suggested that a more robust treatment of the modelled cloud microphysics is needed to improve simulations. Models with less sophisticated microphysics may prescribe a ratio of liquid to ice mass that is inconsistent with Arctic observations. However, models with separate prognostic variables for liquid and ice and detailed microphysics may also produce poor simulations (Morrison *et al.*, 2003; Inoue *et al.*, 2006; Prenni *et al.*, 2007; Sandvik *et al.*, 2007). In these models, a more realistic treatment of ice microphysics, and in particular the number concentration of both small ice and snow, may be needed to improve results. Numerous modelling studies have demonstrated a strong sensitivity of mixed-phase clouds to ice crystal number concentration (Pinto, 1998; Harrington *et al.*, 1999; Jiang *et al.*, 2000; Morrison and Pinto, 2006; Prenni *et al.*, 2007). Prenni *et al.* (2007) substantially improved their simulation of mixed-phase clouds by reducing ice nuclei number concentrations, which influence ice crystal number concentrations, from values typical of midlatitudes to the low values observed in the Arctic. Their simulation was also sensitive to the representation of scavenging of ice nuclei by ice precipitation. Morrison and Pinto (2006) improved their simulation of Arctic mixed-phase stratus by reducing the specified intercept parameter of the snow size distribution; this is equivalent to reducing the snow number concentration for a given snow mixing ratio. These results increase the importance of resolving the long-standing uncertainty in the primary ice formation mechanisms in these clouds (Fridlind *et al.*, 2007). Mixed-phase clouds may also be difficult to represent in large-scale models because their spatial scale may be smaller than the model grid spacing (Field *et al.*, 2004). Several studies have suggested the role of small-scale (turbulent) updraughts in generating and maintaining regions of liquid water in these clouds (Mazin, 1986; Korolev and Isaac, 2003; Korolev and Field, 2008).

To further our understanding of Arctic mixed-phase cloud processes and provide a detailed observational dataset for model evaluation, ARM conducted the Mixed-Phase Arctic Cloud Experiment (M-PACE: Verlinde *et al.*, 2007) over northern Alaska and the adjacent Arctic Ocean during September and October 2004. During M-PACE, a suite of *in situ* and remote sensors gathered measurements of mixed-phase cloud microphysics, dynamics, radiation and aerosol. Already, several studies have used M-PACE observations to assess single-column, cloud-resolving, mesoscale, weather and climate model simulations of mixed-phase clouds (Xie *et al.*, 2006, 2008; Fridlind *et al.*, 2007; Liu *et al.*, 2007b; Prenni *et al.*, 2007; Luo *et al.*, 2008a, 2008b; Morrison *et al.*, 2008).

Given the impact of Arctic clouds on the surface radiation budget and the potential for significant climate feedbacks between sea-ice and clouds, it is vitally important that the representation of these clouds in weather-forecasting and climate models be improved. The Global Energy and Water Experiment Cloud Systems Study (GCSS) project (Randall *et al.*, 2003) recognized this importance by devoting one of its working groups to the study of polar clouds. The GCSS project aims to improve the simulation of important cloud types in weather and climate models by bringing together the expertise of cloud-resolving modellers who study detailed cloud processes with that of large-scale modellers who develop parametrizations for these processes. A central activity of the GCSS project is the intercomparison study in which an observed case is simulated by cloud-resolving models (CRMs) and single-column models (SCMs), and model

DOI: 10.1002/qj

results compared to observations. Indeed, new cloud parametrizations for both cloud-resolving and large-scale models are often first developed in and tested with simulations of GCSS intercomparison case-studies.

This work presents results of the first GCSS intercomparison case-study of the Polar Cloud Working Group. This study involved simulations of mixed-phase clouds observed during two periods in M-PACE and was performed jointly with the ARM Cloud Modeling Working Group. The current paper, Part I, examines results for a single-layer mixed-phase stratocumulus cloud. The accompanying paper, Part II (Morrison *et al.*, 2009), examines results for a deeper, multilayered mixed-phase cloud. These two periods were selected because single-layer mixed-phase boundary layer clouds and multilayer mixed-phase clouds are two commonly occurring Arctic cloud types. Furthermore, cloud processes for single and multilayered clouds may be different.

The goal of this first intercomparison study is to document the current state of model simulations of Arctic mixed-phase clouds and to suggest future areas of work which the Polar Cloud Working Group may use to understand model differences and develop recommendations for model parametrizations. This study presents the range of results and identifies common problems for the widest group of models possible, with the same initial and boundary conditions applied for each period to all simulations. The wide range of participating models allows for a better generalization of results than was previously achieved in the model simulation studies cited above. Although it is not the goal of this study to completely understand model differences, a daunting task given the large number of models and their complexities, a few sensitivity studies are performed to gain some insight into these differences. Other GCSS intercomparison studies have been valuable in identifying important deficiencies in large-scale models such as an underestimate of downdraught mass-fluxes associated with precipitating deep convection over land (Xie *et al.*, 2002) and errors in the simulation of precipitation evaporation from drizzling marine stratocumulus clouds (Wyant *et al.*, 2007).

The next section describes the synoptic situation for the single-layer mixed-phase stratocumulus that is the subject of this paper. Section 3 describes cloud property observations from the *in situ* and ground-based remote sensors that are used to assess model simulations. Section 4 details case specifications while section 5 describes the 17 SCMs and 9 CRMs that participated in the intercomparison. Section 6 compares model simulations to the available observations and section 7 describes the results of two sensitivity studies. Section 8 briefly summarizes the key findings.

2. Synoptic situation

The boundary layer cloud system that is the focus of this study occurred during a period of north-easterly flow around an anticyclone to the north of Alaska (Verlinde *et al.*, 2007). As cold air to the northeast of Alaska flowed off the sea ice and over the open ocean adjacent to the coast, significant surface heat fluxes of temperature and water vapour induced the formation of boundary layer clouds in the form of 'rolls' or 'cloud-streets' which are common in 'cold-air outbreak' stratocumulus (Figure 1). With the surface forcing, the boundary layer, as observed at the Alaska coast, was 'well-mixed'. This was demonstrated by the fact that the vertical profiles of water vapour and potential temperature match those in which the variables of water and energy that are conserved during the condensation process are uniform in the boundary layer (Figure 2).

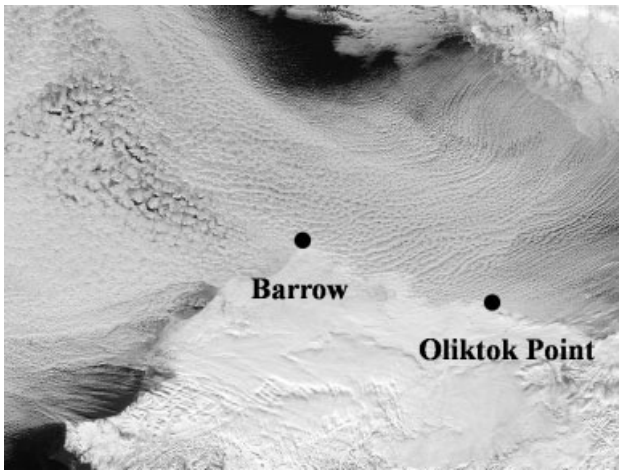

Figure 1. Moderate resolution imaging spectroradiometer composite visible image of northern Alaska and the Beaufort Sea for 9 October 2004. The boundary-layer clouds occurred when cold air above the sea ice to the northeast of Alaska flowed over the ice-free Beaufort Sea inducing significant surface heat fluxes responsible for cloud formation. The sea ice is visible in the upper right corner of the image. The clouds were observed in the north-easterly flow between the ARM stations of Barrow and Oliktok Point on the coast of snow-covered Alaska. As is common in 'cold-air outbreak' stratocumulus, boundary-layer 'rolls' or 'cloud streets' developed with a horizontal scale that increases in the downstream direction.

During the focus period for this study, 1700 UTC 9 October to 0500 UTC 10 October 2004, the boundary layer was between 1000 and 1500 m deep at the coast of Alaska. As observed by both aircraft and ground-based remote sensors, the upper half of the boundary layer contained a mixed-phase cloud with a cloud-top temperature of about -15°C. This cloud contained an amount of liquid water which in terms of condensate mass far exceeded the amount of ice present in the cloud. Beneath the cloud base, which is identified here as the lowest level to contain liquid water, ice crystal precipitation occurred that reached the surface. The boundary layer was capped by a weak inversion of about 2 K with dry and cloudless skies above.

3. Cloud observations

3.1. Aircraft observations

During this period, there were two flights of the University of North Dakota Citation (McFarquhar *et al.*, 2007a). The Citation performed a number of spirals above Barrow

DOI: 10.1002/qj

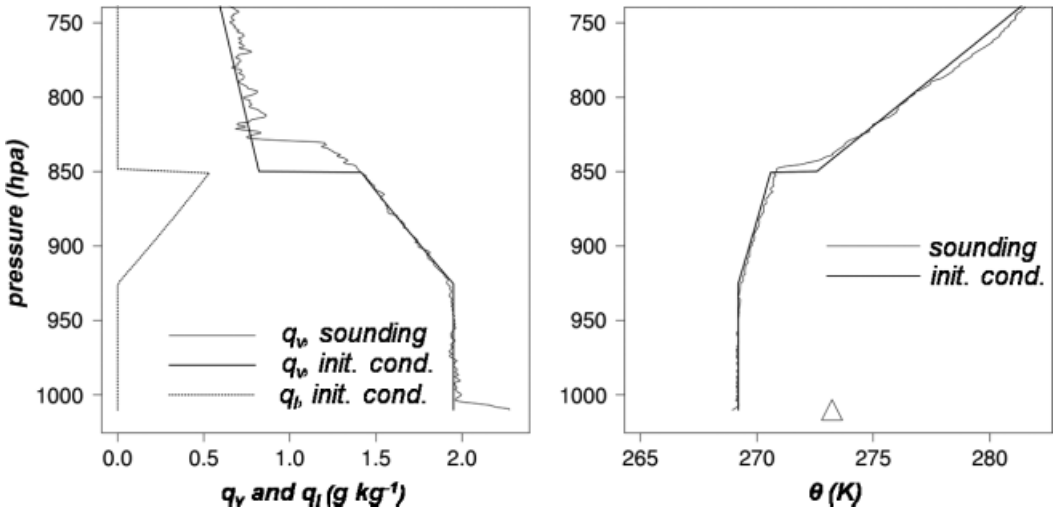

Figure 2. Initial conditions for model simulations of the potential temperature (right panel, thick line) and mixing ratios of water vapour (left panel, thick line) and cloud liquid (left panel, dotted line). Also shown are the values of the potential temperature (right panel, thin line) and water vapour mixing ratio (left panel, thin line) from the 1700 UTC 9 October 2004 sounding at Barrow. The triangle in the right panel indicates the value of the ocean surface potential temperature in the coastal region.

and Oliktok Point as well as ramped ascents or descents along the coastline between the two stations. From the two flights, there are a total of 32 vertical profiles which are analysed in this study.

On board were probes that nominally measured the size distribution of particles with maximum dimensions (D) between 3 μm and 40 mm, as well as the total condensate and liquid water contents separately. Interpretation of data from these probes is non-trivial and subject to uncertainties. Information on phase, size distribution, and bulk microphysical parameters are from the analysis of McFarquhar *et al.* (2007a) who describe a methodology for intercomparison and interpretation of the aircraft data. Cloud phase was determined to be either liquid only, ice only or mixed-phase, from an algorithm that considered output of an icing detector, visual inspection of particle images, and the shape of the particle size distribution. The phase classification was made for each 30 s flight segment with total water content greater than 0.001 g m^{-3} (Fig. 2 of McFarquhar *et al.*, 2007a). A 30 s segment corresponds approximately to 2500 m of horizontal distance.

In addition to phase, calculated bulk parameters include liquid and ice water contents as well as particle number concentration and effective radius determined separately for liquid and ice in each 30 s segment. Ice parameters correspond only to particles with $D > 53$ μm because the characteristics of smaller ice crystals contain very large measurement uncertainties due to potential shattering of large ice crystals on the inlets and protruding shrouds of probes used to measure small ice crystals (McFarquhar *et al.*, 2007b). Particles with $D < 0.125$ mm measured by the two-dimensional cloud probe are not used because previous studies have suggested that there are problems with quantifying concentrations in this size range (Baumgardner and Korolev, 1997; Strapp *et al.*, 2001). The one-dimensional cloud probe is used, albeit with large uncertainty, to provide the concentration of particles between 0.05 and 0.125 mm. It should be noted that McFarquhar *et al.* (2007a) showed that the majority of particles with $D > 53$ μm are ice because a statistical analysis of cloud particle imager observations suggested that only 19% of observations in mixed-phase conditions had at least one drizzle particle. However, there were a few occasions where circular cloud particle images suggest that supercooled drizzle with $D > 53$ μm is present beneath cloud base. For these occasions, particles with $53 < D < 125$ μm were assumed to be liquid.

McFarquhar *et al.* (2007a) describe the uncertainties in the derived bulk parameters. Because the mixed-phase clouds are dominated by contributions of supercooled water, rough estimates of uncertainty are ±15% for the bulk liquid parameters due to uncertainties in the King probe. A factor-of-two uncertainty exists for the bulk ice parameters in ice-only regions, mainly due to uncertainties in the mass–D relationship used for ice particles. The minimum detectable water content is on the order of 0.001 g m^{-3} (McFarquhar *et al.*, 2007a). However, because Cober *et al.* (2001) noted that the minimum detectable water content of the Rosemount icing detector was 0.007 g m^{-3} and because the spectral shape of the forward scattering spectrometer probe is likely not peaked for the occurrence of supercooled drizzle, it is plausible that some instances of supercooled water were not identified by McFarquhar *et al.* (2007a) and that the minimum detectable supercooled water content is on the order of 0.01 g m^{-3}.

3.2. Ground-based remote sensor observations

Cloud physical and dynamical properties and surface radiative fluxes have been retrieved from the active and passive sensors deployed at Barrow and Oliktok Point. Two sets of mixed-phase cloud retrievals are available (Wang and Sassen, 2002; Turner, 2005; Shupe *et al.*, 2006; Shupe, 2007; Turner *et al.*, 2007; Wang, 2007, hereafter termed WANG; Shupe *et al.*, 2008, hereafter

DOI: 10.1002/qj

termed SHUPE-TURNER). The retrievals primarily rely on measurements from the millimetre wavelength cloud radar, lidar, and microwave radiometer. Except for liquid water path, cloud property retrievals are available only at Barrow.

Retrieved cloud physical properties include cloud top and base, cloud phase, the vertical profiles and vertically integrated amounts of liquid and ice water content, and the effective particle sizes of liquid and ice. Using a multi-sensor approach, Shupe (2007) derives a cloud phase mask that distinguishes target volumes into ice, liquid, mixed-phase or clear categories. Although vertical profiles of liquid water content can be derived by scaling an assumed adiabatic liquid water profile to the observed liquid water path, in this study models are compared only to the microwave radiometer liquid water path of which two estimates are available (Turner *et al.*, 2007, hereafter termed TURNER; WANG). Cloud ice properties are derived from seasonally-tuned radar retrievals (Shupe *et al.*, 2006) or from a combined radar–lidar method (Wang and Sassen, 2002). For this case-study, rough uncertainty estimates are 20 g m^{-2} for the liquid water path (TURNER) and a factor of two for the ice water content and path (Shupe *et al.*, 2006). Based upon the radar minimum detectable signal of −50 dBZ, the minimum detectable ice water content is on the order of 0.002 g m^{-3}. The time resolution of the remote sensing data is approximately 1 min which corresponds to a horizontal wind-advection distance of 800 m.

4. Case specifications

Because of the role of ocean surface fluxes in cloud formation, it was assumed that models were above an ocean surface with forcing specified in the manner of previous GCSS boundary layer cloud working group intercomparisons (Stevens *et al.*, 2005; Zhu *et al.*, 2005). The initial condition for all models was a cloud-topped boundary layer that was well-mixed and capped by an inversion. In terms of the ice–liquid-water potential temperature θ_{li} and total water mixing ratio q_t which are conserved variables under adiabatic conditions, these initial conditions were specified as:

$$\theta_{li} = \begin{cases} 269.2\ \text{K} & \text{for } p > p_{inv} \\ 275.33\ \text{K} + 0.0791\ \text{K hPa}^{-1} \times (815\ \text{hPa} - p) & \text{for } p < p_{inv} \end{cases} \quad (1)$$

$$q_t = \begin{cases} 1.95\ \text{g kg}^{-1} & \text{for } p > p_{inv} \\ 0.291\ \text{g kg}^{-1} + 0.00204\ \text{g kg}^{-1}\ \text{hPa}^{-1} \times (p - 590\ \text{hPa}) & \text{for } p < p_{inv} \end{cases} \quad (2)$$

where p is atmospheric pressure and p_{inv} is the inversion pressure with a value of 850 hPa. The total water mixing ratio q_t is defined as $q_t = q_v + q_l + q_i$, where q_v, q_l and q_i are the mixing ratios of water vapour, liquid water and ice water, respectively. The definition of θ_{li} used here is:

$$\theta_{li} = T \times (p_0/p)^{R_d/c_p} \times \exp\{-(L_v q_l + L_s q_i)/c_p T_{cb}\} \quad (3)$$

where T is the absolute temperature, p_0 is a reference pressure of 1000 hPa, T_{cb} is the cloud base temperature of 263 K, R_d is the dry air gas constant, c_p is the specific heat capacity of dry air at constant pressure, and L_v and L_s are the latent heats of vaporization and sublimation, respectively. Figure 2 displays the initial conditions of the potential temperature and the mixing ratios of water vapour and liquid water which are consistent with (1) and (2).

Note that the initial phase of the cloud was specified to be pure liquid. It was assumed that the microphysics present in the model would develop ice during the simulation and that a microphysical steady state would occur after a few hours of model spin-up. The lower boundary condition was specified as an ocean surface with temperature 274.01 K. Models were asked to simulate the 12 h starting from 1700 UTC 9 October 2004.

For advective forcing of models in an Eulerian system, one must specify the horizontal advection of temperature and water vapour as well as the vertical velocity, from which models can calculate the vertical advection of temperature and water vapour. These forcings were based upon analysis data from the European Centre for Medium-Range Weather Forecasts (ECMWF) for the ocean region 200 km upstream from the coastline between Barrow and Oliktok Point. ECMWF data for these forcings were idealized to:

$$-\mathbf{V} \bullet \nabla T = \min(-4, -15 \times [1 - \{(p_s - p)/218.18\ \text{hPa}\}])\quad \text{K day}^{-1} \quad (4)$$

$$-\mathbf{V} \bullet \nabla q_v = \min(-0.164, -3 \times [1 - \{(p_s - p)/151.71\ \text{hPa}\}])\ \text{g kg}^{-1}\text{day}^{-1} \quad (5)$$

$$\omega = \min\{D \times (p_s - p), D \times (p_s - p_{inv})\} \quad (6)$$

where $-\mathbf{V} \bullet \nabla T$ is the temperature tendency from horizontal advection, $-\mathbf{V} \bullet \nabla q_v$ is the mixing ratio tendency from horizontal advection, and ω is the vertical pressure velocity (Figure 3). In these equations, p_s is the surface pressure and D is the large-scale divergence with values of 1010 hPa and 5.8×10^{-6} s^{-1}, respectively. This idealization of the ECMWF data was made in order to have vertically smooth forcing profiles that minimize drifts in the temperature and water vapour above the boundary layer.

Lacking *in situ* observations and in order to minimize model differences, surface fluxes are specified from ECMWF data with values of 136.5 W m^{-2} for sensible heat and 107.7 W m^{-2} for latent heat. While significant uncertainties exist regarding the actual magnitudes

DOI: 10.1002/qj

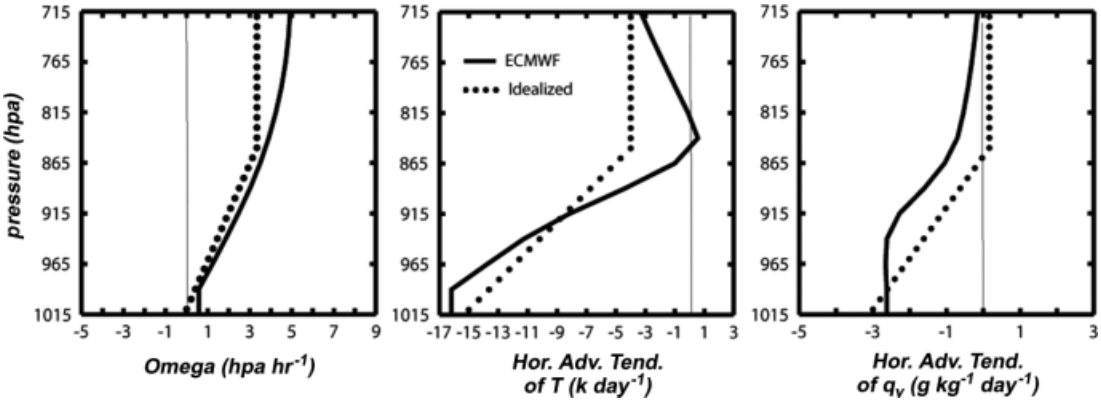

Figure 3. Vertical pressure velocity (Omega) and the horizontal advective tendencies of temperature and water vapour mixing ratio for the period 1700 UTC 9 October to 0500 UTC 10 October 2004. Each panel displays the values from the ECMWF analysis (solid line) and the values used in the model simulations (dots).

of these fluxes, sensitivities studies altering these fluxes by ±25% in the UCLA-LARC CRM alter the simulated liquid and ice water paths by up to 30% and 50%, respectively (Luo *et al.*, 2008a). These differences are smaller than differences among models and between models and observations, as shown below. The surface fluxes imply a turbulent boundary layer as the convective velocity scale (Stull, 1988, p 355) is approximately 1 m s^{-1}. Furthermore, radiation calculations with the observed cloud (section 6.7) suggest that there is a significant long-wave radiative cooling of 70 W m^{-2} at cloud top. With turbulence being forced from the top and bottom of the boundary layer, it is not surprising that thermodynamic profiles in the boundary layer are approximately well-mixed. One confirmation of the turbulent nature of the boundary layer is that the SHUPE-TURNER cloud radar retrievals indicate that the interquartile range of vertical velocity inside the cloud is 0.8 m s^{-1} (Fig. 5c of Shupe *et al.*, 2008).

Besides buoyancy forcing from the top and bottom of the boundary layer, strong horizontal winds were present which imply a significant surface stress which also induces mixing. Models were asked to maintain the mean boundary layer wind close to the observed values of -13 m s^{-1} in the zonal direction and -3 m s^{-1} in meridional direction and most models used nudging to accomplish this.

Radiation calculations in both the solar and long-wave portion of the spectrum were performed by each model using their own predicted atmospheric state and radiation parametrization. Calculated radiative heating rates affect the evolution of the atmosphere and in particular, cloud-top radiative cooling can drive atmospheric circulations. Surface radiative fluxes do not affect surface temperatures, because the surface temperature and heat fluxes are specified. However, these radiative fluxes are compared with observations to assess the fidelity of model simulations.

The following aerosol characteristics, more fully discussed in Morrison *et al.* (2008), were recommended for models that have an explicit aerosol–cloud coupling. For the aerosol size distribution, a bimodal log-normal dry aerosol size distribution was fitted to available observations. The size distribution for each mode is given by

$$\frac{\mathrm{d}N}{\mathrm{d}\ln r} = \frac{N_\mathrm{t}}{\sqrt{2\pi}\ln\sigma}\exp\left\{-\frac{\ln^2(r/r_\mathrm{m})}{2\ln^2\sigma}\right\} \qquad (7)$$

where N is the number concentration of aerosols and r is the particle radius. The parameters N_t, r_m and σ are total number concentration, geometric mean radius and standard deviation of each particle mode. For the smaller particle mode, these parameters have values of 72.2 cm^{-3}, 0.052 μm and 2.04, respectively. For the larger particle mode, these parameters have values of 1.8 cm^{-3}, 1.3 μm and 2.5, respectively. Aerosol composition was assumed to be ammonium bisulphate with an insoluble fraction of about 30%.

The number concentration of ice nuclei is an important parameter for models that simulate the number concentration of ice crystals. The Continuous Flow Diffusion Chamber on the Citation measured ice nuclei with a diameter less than 2 μm acting in deposition, condensation-freezing, and immersion-freezing modes (Prenni *et al.*, 2007). No measurement of ice nuclei acting in contact mode was possible. Measurements indicate extremely low amounts of ice nuclei, with 85% of measurements having ice nuclei beneath background levels of 0.1 L^{-1} (Verlinde *et al.*, 2007). Of the measurements with ice nuclei above background, the maximum concentration was about 10 L^{-1}. The mean of all observations including those beneath background levels was 0.16 L^{-1}, which was the recommended value for models.

More information on the intercomparison specifications and plots of model simulations and observational data are available from http://science.arm.gov/wg/cpm/scm/scmic5/index.html.

5. Model descriptions

5.1. Overview

Tables I and II encapsulate the relevant characteristics of the 17 SCMs and 9 CRMs that took part in this intercomparison.

DOI: 10.1002/qj

Table I. Characteristics of participating single-column models.

Model	Investigator and Model reference	Cloud microphysics	Prognostic cloud variables	Do clouds depend on aerosols?	No. of vertical levels in the PBL at std (high) resolution
ARCSCM	Hugh Morrison *Morrison* et al. *(2003)*	double moment *Morrison* et al. *(2005a)*	q_l q_i q_r q_s N_l N_i N_s N_r	Yes	10 (20)
CCCMA	Jason Cole Knut von Salzen *von Salzen (2006)*	single moment with independent liquid and ice *von Salzen (2006)*	q_l q_i	Yes (liquid only)	10 (16)
ECHAM	Corinna Hoose *Roeckner* et al. *(2003)*	double moment *Lohmann* et al. *(2007)*	q_l q_i N_l N_i	Yes	6 (23)
ECMWF	Roel Neggers *ECMWF (2007)*	single moment with T-dependent partitioning (12% liquid at −15°C) *ECMWF (2007)*	q_c	No	14
ECMWF-DUALM	Roel Neggers *Neggers* et al. *(2009)*	single moment with T-dependent partitioning (12% liquid at −15°C) *ECMWF (2007)*	q_c	No	14
GFDL	Stephen Klein *GFDL GAMDT (2004)*	single moment with independent liquid and ice *Rotstayn* et al. *(2000)*	q_l q_i	No	9 (34)
GISS	Audrey Wolf Anthony DelGenio *Hansen* et al. *(2002)*	single moment with independent liquid and ice *Schmidt* et al. *(2006)*	q_l q_i	No	6
GISS-LBL	Igor Sednev Surabi Menon *Hansen* et al. *(2002)*	bin microphysics *Khain and Sednev (1996)*	33 bins each for liquid droplets, plates, columns, dendrites, snow, graupel, and frozen drops	Yes	8
MCRAS	Yogesh Sud Gregory Walker *Sud and Lee (2007)*	single moment with T-dependent partitioning (75% liquid at −15°C) *Sud and Lee (2007)*	q_c N_l	Yes (liquid only)	4 (15)

DOI: 10.1002/qj

Table I. *Continued.*

Model	Investigator and Model reference	Cloud microphysics	Prognostic cloud variables	Do clouds depend on aerosols?	No. of vertical levels in the PBL at std (high) resolution
MCRASI	Yogesh Sud Gregory Walker *Sud and Lee (2007)*	double moment *Liu and Penner (2005)*	q_l q_i N_l N_i	Yes	4 (15)
NCEP	Fanglin Yang *EMC (2003)*	Single moment with T-dependent partitioning (25% liquid at −15°C) *Zhao and Carr (1997)*	q_c	No	12 (128)
SCAM3	Shaocheng Xie *Collins* et al. *(2006)*	single moment with T-dependent partitioning (83% liquid at −15°C) *Boville* et al. *(2006)*	q_c	No	4 (14)
SCAM3-LIU	Xiaohong Liu *Collins* et al. *(2006)*	double moment *Liu* et al. *(2007a)*	q_l q_i N_l N_i	Yes	4 (14)
SCAM3-MG	Hugh Morrison *Collins* et al. *(2006)*	double moment *Morrison and Gettelman (2008)*	q_l q_i N_l N_i	Yes	4
SCAM3-UW	Sungsu Park *Bretherton and Park (2009)*	single moment with T-dependent partitioning (83% liquid at −15°C) *Boville* et al. *(2006)*	q_c	No	7 (125)
SCRIPPS	Michael Foster Dana Veron *Iacobellis and Somerville (2006)*	single moment with independent liquid and ice *Rotstayn (1997)*	q_l q_i	No	7 (17)
UWM	Michael Falk Vincent Larson *Golaz* et al. *(2002)*	single moment with independent liquid and ice *Larson* et al. *(2006)*	q_l q_i	No	51 (146)

For prognostic cloud variables, q_l, q_i, q_r, q_s and q_g are the mixing ratio of cloud liquid, cloud ice, rain, snow and graupel, respectively. q_c is the mixing ratio of cloud condensate and is equal to the sum of q_l and q_i. N_l, N_i, N_r, N_s and N_g are the number concentrations of cloud liquid, cloud ice, snow and graupel, respectively. In the table, T, PBL, and std are abbreviations for temperature, planetary boundary layer and standard, respectively. For purposes of this table, the height of the planetary boundary layer is defined as 1350 m.

DOI: 10.1002/qj

Table II. As in Table I but for participating cloud-resolving models.

Model	Investigator and Model reference	Cloud microphysics	Prognostic cloud variables	Do clouds depend on aerosols?	Dimensionality, Horizontal (std vertical) resolution, Domain size	No. of vertical levels in the PBL at std (high) resolution
COAMPS®	Jean-Christophe Golaz Jerome Schmidt *Golaz et al. (2005)*	Double moment *Chen et al. (2003)*	q_l q_i q_r q_s q_g N_l N_i N_r	No	3D 50m (20m) 4.8km by 4.8km	67
DHARMA	Ann Fridlind Andy Ackerman *Ackerman et al. (2004)*	bin microphysics *Fridlind et al. (2007)*	20 liquid, 20 ice, and 10 ice nuclei bins	Yes	3D 50m (21m) 3.2km by 3.2km	64
METO	Ben Shipway *Shutts and Gray (1994)*	Double moment *Ferrier (1994)*	q_l q_i q_r q_s q_g N_i N_s N_g	No	3D 50m (50m) 6.4km by 6.4km	27 (53)
NMS-BULK	Gijs deBoer Tempei Hashino *Tripoli (1992)*	Double moment *Flatau et al. (1989)*	q_l q_i q_r q_s q_g N_l N_i N_r N_s N_g	No	2D 200m (100m) 60 km	13
NMS-SHIPS	Gijs deBoer Tempei Hashino *Tripoli (1992)*	bin microphysics *Hashino and Tripoli (2007)*	21 liquid, 20 ice and 1 aerosol bins	Yes (ice only)	2D 200m (100m) 60 km	13
RAMS-CSU	Alex Avramov Jerry Harrington *Cotton et al. (2003)*	Double moment *Meyers et al. (1997)*	q_l q_i q_r q_s q_g N_l N_i N_s N_g	Yes (ice only)	2D 1000m (70m) 150 km	17 (29)
SAM	Mingxuan Chen Marat Khairoutdinov *Khairoutdinov and Randall (2003)*	single moment with T-dependent partitioning (25% liquid at −15°C) *Khairoutdinov and Randall (2003)*	q_c q_p	No	3D 100m (50m) 12.7km by 12.7km	27 (53)
UCLA-LARC	Yali Luo Kuan-Man Xu *Luo et al. (2008a)*	Double moment *Morrison et al. (2005a)*	q_l q_i q_r q_s N_l N_i N_r N_s	Yes	2D 2km (180m) 256 km	7 (23)
UCLA-LARC-LIN	Yali Luo Kuan-Man Xu *Xu and Krueger (1991)*	single moment with independent liquid and ice *Lin et al. (1983)*	q_l q_i q_r q_s q_g	No	2D 2km (180m) 256 km	7 (23)

The dimensionality of the model is listed as two-dimensional (2D) or three-dimensional (3D). q_p is the mixing ratio of precipitating condensate and is equal to the sum of q_r, q_s and q_g.

DOI: 10.1002/qj

Among SCMs, there are versions of two operational weather prediction models (ECMWF and NCEP) and five operational climate models (CCCMA, ECHAM, GFDL, GISS, and SCAM3). There are four SCMs which have primarily been used in research studies (ARCSCM, MCRAS, SCRIPPS, and UWM). Finally, there are six SCMs which include single modifications of the base set of SCMs (ECMWF-DUALM, GISS-LBL, MCRASI, SCAM3-LIU, SCAM3-MG, and SCAM3-UW). Four of these six include modifications to the representation of cloud microphysics: three SCMs add double-moment microphysics (MCRASI, SCAM3-LIU, and SCAM3-MG) and one adds bin resolved cloud microphysics (GISS-LBL). Two of these six include modifications to the representation of boundary layer turbulence (ECMWF-DUALM and SCAM3-UW). The number of vertical levels in the boundary layer varies from four to 51 with a median value of seven.

Among CRMs, five are two-dimensional (NMS-BULK, NMS-SHIPS, RAMS-CSU, UCLA-LARC, UCLA-LARC-LIN), and four are three-dimensional (COAMPS®, DHARMA, METO, and SAM). There is a wide variety of horizontal and vertical resolutions as well as total domain represented. The two-dimensional models typically have horizontal and vertical resolutions of order 1000 m and 100 m, respectively, whereas the three-dimensional models typically have horizontal and vertical resolutions of 50 m in both directions. The number of vertical levels in the boundary layer varies from 7 to 17 for the two-dimensional models and from 27 to 67 for the three-dimensional models. Total domain size is of order 100 km for the two-dimensional models and 5000 m by 5000 m for the three-dimensional models. Thus, configurations of the two-dimensional models are typical of models commonly referred to as 'cloud-resolving models' whereas configurations of the three-dimensional models are typical of models commonly referred to as 'large-eddy simulations'.

5.2. Cloud microphysics

As the representation of cloud microphysics may be central to the ability of models to simulate a mixed-phase cloud, a summary of the microphysics used in these models is now given. Readers seeking more detail should consult the references in Tables I and II.

The parametrizations of cloud microphysics can be classified into four categories which span the range of detail used in today's cloud models. The simplest representation, which will be called 'single-moment with T-dependent partitioning', employs a single prognostic variable for the mass of cloud condensate and uses a temperature-dependent function to partition the relative amounts of liquid and ice. The relative amount of liquid at the cloud-top temperature of -15°C varies from 12% to 83% in the six SCMs (ECMWF, ECMWF-DUALM, MCRAS, NCEP, SCAM3, SCAM3-UW) and one CRM (SAM) that have this type of microphysical representation. Note that SAM also employs a temperature-dependent partitioning to determine the relative amounts of rain, snow and graupel which at -15°C are 0%, 42% and 58%, respectively.

The second class of cloud microphysics, 'single-moment with independent liquid and ice', employs separate prognostic variables for the mass of cloud liquid and ice in which relative amounts of liquid and ice are not solely a function of temperature. Five SCMs (CCCMA, GFDL, GISS, SCRIPPS, and UWM) and one CRM (UCLA-LARC-LIN) employ this class of microphysics. Considerations which determine the relative amounts of liquid and ice in these models typically include a temperature-dependent partitioning of liquid and ice at cloud formation and subsequent conversion of liquid to ice through riming, droplet freezing, or the Bergeron–Findeisen process which in mixed-phase clouds favours the growth of ice over liquid due to ice's lower saturation vapour pressure.

The third class of cloud microphysics, 'double-moment', employs prognostic variables for both the mass of condensate as well as the number concentration of cloud particles. Five SCMs (ARCSCM, ECHAM, MCRASI, SCAM3-LIU, SCAM3-MG) and five CRMs (COAMPS®, METO, NMS-BULK, RAMS-CSU, UCLA-LARC) employ this approach. An advantage over the previous two classes is that a prognostic representation of number concentration potentially allows for a physically based coupling of clouds with aerosols. While not every condensate species may be represented with a prognostic variable for number concentration, all double-moment parametrizations in this study represent the number concentration of cloud (or small) ice with a prognostic variable.

The fourth class of cloud microphysics, 'bin microphysics', represents the number concentration of particles of different sizes with prognostic variables. This is the most complete representation of microphysics used in this study and is used in one SCM (GISS-LBL) and two CRMs (DHARMA and NMS-SHIPS). In DHARMA and NMS-SHIPS, 20 size bins each are used to represent liquid and ice particles. DHARMA has 40 additional size bins for the mass of dissolved solute in each of the liquid drop and ice crystal size bins. GISS-LBL uses 33 size bins to represent liquid droplets and six classes of solid or partially solid condensate which include plates, columns, dendrites, snow, graupel, and frozen drops.

In general, only models with double-moment or bin microphysics represent the dependence of cloud properties on aerosols. However, three models with double-moment parametrizations do not have an explicit dependence of cloud properties on aerosols (COAMPS®, METO, NMS-BULK). Of the 12 models in which cloud properties depend on aerosols (ARCSCM, CCCMA, DHARMA, ECHAM, GISS-LBL, MCRAS, MCRASI, NMS-SHIPS, RAMS-CSU, SCAM3-LIU, SCAM3-MG, UCLA-LARC), two models couple only the liquid-phase microphysics (CCCMA and MCRAS) while two others couple only the ice-phase microphysics (NMS-SHIPS and RAMS-CSU).

DOI: 10.1002/qj

Further discussion of the widely-varying treatment of ice microphysics in models is warranted because previous studies have demonstrated the critical importance of ice microphysics in simulations of Arctic mixed-phase clouds, especially representation of the vapour depositional growth of ice and the Bergeron–Findeisen process (Harrington *et al.*, 1999; Morrison and Pinto, 2006; Prenni *et al.*, 2007). Single-moment schemes with T-dependent partitioning do not explicitly treat ice initiation and conversion of cloud liquid water to ice, and instead fix the ratio of liquid and ice as a function of temperature. Most of the single-moment schemes with independent liquid and ice and all of the two-moment and bin schemes explicitly represent the Bergeron–Findeisen process and most include additional liquid–ice conversion processes via heterogeneous droplet freezing. In the more detailed one-moment schemes (GFDL, UCLA-LARC-LIN, UWM) and all of the bin and two-moment schemes except that of ECHAM, the Bergeron–Findeisen process depends on the specified or predicted ice crystal number concentration as well as other ice microphysical parameters (e.g. capacitance). It is this dependence that has led to significant sensitivity of mixed-phase cloud simulations to treatment of ice crystal number concentration in previous studies (Pinto, 1998; Harrington *et al.*, 1999; Jiang *et al.*, 2000; Morrison *et al.*, 2003; Morrison and Pinto, 2006; Prenni *et al.*, 2007).

The ice crystal number concentration is specified in single-moment schemes, and this specification varies widely among participating models. In two-moment and bin schemes, the ice crystal number concentration is predicted and evolves through various source (primary ice nucleation and secondary ice multiplication) and sink (aggregation, sedimentation) terms. In all simulations presented here, primary ice nucleation is the dominant source, and secondary ice multiplication is of limited importance. Ice nucleation occurs via several mechanisms including contact and immersion freezing, deposition, and condensation-freezing, although their representation differs widely among models. Most models treat ice nuclei concentration diagnostically, although two models (DHARMA and RAMS-CSU) prognosticate this quantity. Several models with diagnostic ice nuclei scale their values to those observed in M-PACE (ARCSCM, ECHAM, GISS-LBL, NMS-BULK, SCAM-MG, UCLA-LARC). However, other models used their default ice nuclei concentrations, such as the formulation from Meyers *et al.* (1992) which predicts amounts far greater than observed. Even among models that scaled their ice nuclei concentrations to observations, this scaling was not applied to all parametrized nucleation mechanisms.

6. Results

6.1. Cloud and hydrometeor fraction

Figure 4 displays the height profile of the average cloud fraction from observations and model simulations. For observations, one profile is from the ground-based remote sensors at Barrow (SHUPE-TURNER) and the other two are from the two aircraft flights. The aircraft cloud fraction depicts the fraction of time in a flight in which a given altitude was between cloud base and cloud top. For the remote sensors, cloud top is defined as the altitude of the highest range gate with significant radar return, and cloud base is defined from the laser ceilometer which corresponds in this case to the lowest altitude with a significant amount of liquid water. For the aircraft, cloud top is defined as the highest altitude with cloud liquid or ice, and cloud base is defined as the lowest altitude with liquid water, where the presence of liquid or ice is determined by the approximate threshold value for detectable water content of 0.001 g m^{-3} (McFarquhar *et al.*, 2007a).

Figure 4 indicates that the cloud bases, tops and thicknesses are greater in the retrievals from ground-based remote sensors at Barrow than they are in those determined from aircraft data. Some of these differences are due to a strong east–west gradient in cloud base, top and thickness observed by the aircraft flying between Oliktok Point and Barrow. For example, easternmost spirals near Oliktok Point in both flights have cloud tops of 950 to 1000 m whereas westernmost spirals near Barrow have cloud tops of 1300 to 1500 m. The east–west gradient in cloud thickness is consistent with the greater liquid water path retrieved from the microwave radiometer at Barrow relative to that of Oliktok Point (Table III). It is also consistent with the satellite image of Figure 1 which shows that the typical roll width, which is generally positively correlated to the depth of the boundary layer, is greater at Barrow than at Oliktok Point.

Similar to the observations, SCMs and CRMs produce a solid cloud layer between 700 and 1300 m (Figure 4). To construct each model cloud fraction plot, the cloud fraction for each model was averaged over the 12 h simulation omitting the first 3 h for model spin-up. From the set of cloud fraction profiles, the values of cloud fraction at each height corresponding to the median, minimum, maximum and 25th and 75th percentiles of models were calculated. The model plots show the median cloud fraction (solid black line), the inner 50% of models (the darker shaded area), and the range of the data (the area of both the lighter and darker shading). All CRMs were asked to compute cloud fraction which was defined as the fraction of grid volumes with cloud droplet mixing ratios greater than 0.01 g kg^{-1} or ice mixing ratios greater than 0.0001 g kg^{-1}. Unfortunately, these thresholds differ from those of the aircraft or ground-based remote sensors (section 3) which were determined at a later time than when this intercomparison began; however, differences in thresholds are not likely to have a great impact on statistics of the cloud and hydrometeor fraction, and have little or no impact on other diagnostics examined in this paper. For SCMs, cloud fraction is an inherent property of the model which generally means the horizontal fraction of a grid cell that is saturated and contains either cloud liquid or ice.

DOI: 10.1002/qj

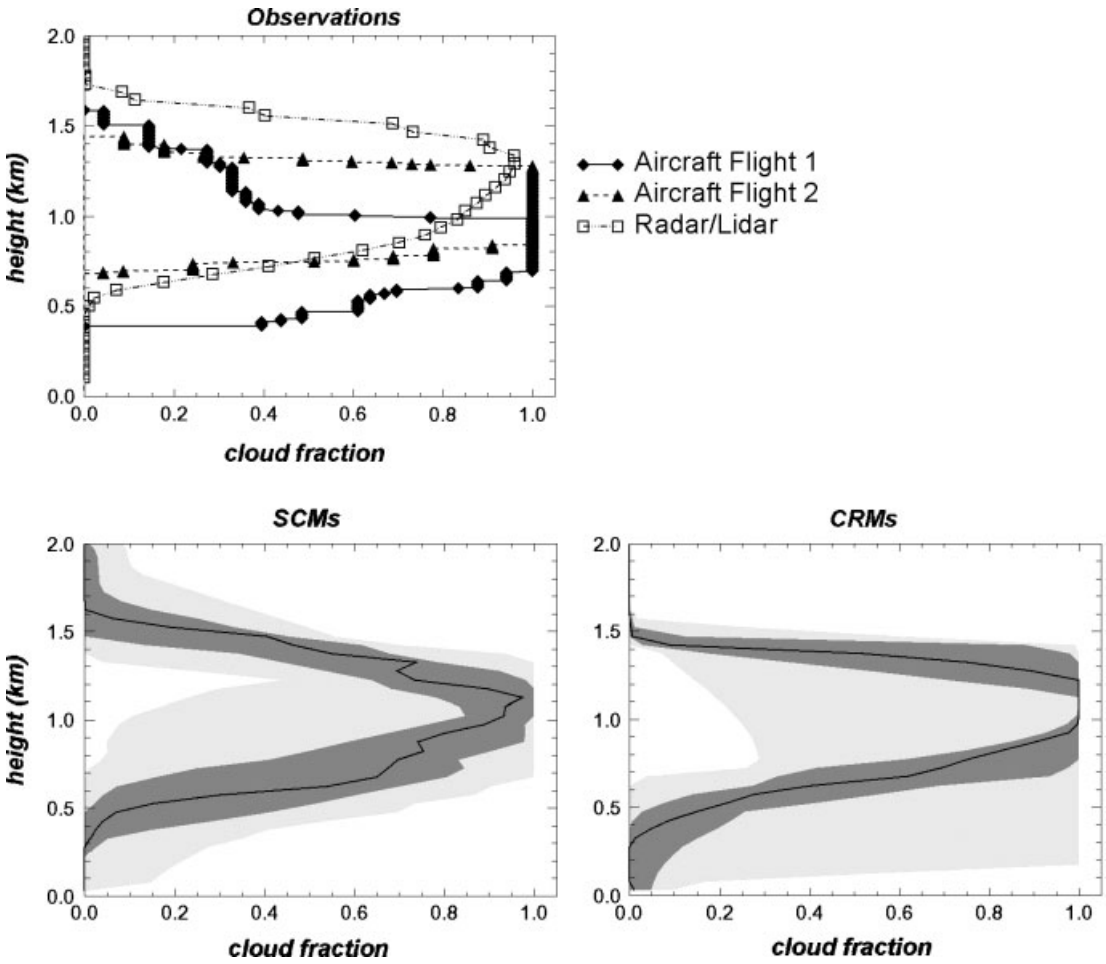

Figure 4. Time-averaged cloud fraction from observations and models as a function of height. The observations panel depicts the fraction of time at each height that cloud was observed from remote sensors at Barrow (SHUPE-TURNER) and the two aircraft flights during the period 1700 UTC 9 October to 0500 UTC 10 October 2004. Model panels depict statistical properties of the mean cloud fraction for hours 4–12 of model simulations. The properties depicted include the median of models (solid black line), the inner 50% of models (dark shading), and the outer 50% of models (light shading).

Table III. Median condensate water paths and interquartile ranges in parentheses from observations for the study period.

	Liquid water path (g m^{-2})	Ice water path (g m^{-2})
Aircraft		
Flight 1009	130.1 (94.2–143.2)	8.0 (4.7–16.4)
Flight 1010a	109.3 (101.2–116.9)	3.5 (2.5–11.7)
Combined flights	115.3 (98.3–135.7)	7.6 (3.4–14.7)
Ground-based		
SHUPE-TURNER @ Barrow	224.2 (172.3–280.8)	30.7 (19.2–42.8)
WANG @ Barrow	195.6 (141.2–251.3)	28.1 (22.3–38.0)
TURNER @ Oliktok Point	87.6 (69.1–103.5)	–
WANG @ Oliktok Point	127.9 (102.0–151.6)	–

Both observed and modelled clouds produced precipitation. This is shown in a plot of the hydrometeor fraction (Figure 5), which is defined as the area fraction which contains either cloud or precipitation. From observations, this was calculated using the presence of any liquid or ice condensate from the remote sensor retrievals. For the models, this was calculated using either the presence of cloud, as defined above, or rain, snow or graupel mixing ratios in excess of 0.0001 g kg^{-1}. The remote sensors indicate that the cloud continually produced precipitation which reached the surface.

As to the hydrometeor phase, classifications from aircraft data and remote sensors (SHUPE-TURNER) are largely consistent (Figure 6). This figure displays the fraction of time that a given phase occurred composited on a normalized height coordinate where -1 is the surface, 0 is cloud base, and $+1$ is cloud top. The observations indicate most of the cloud is mixed-phase (liquid and

DOI: 10.1002/qj

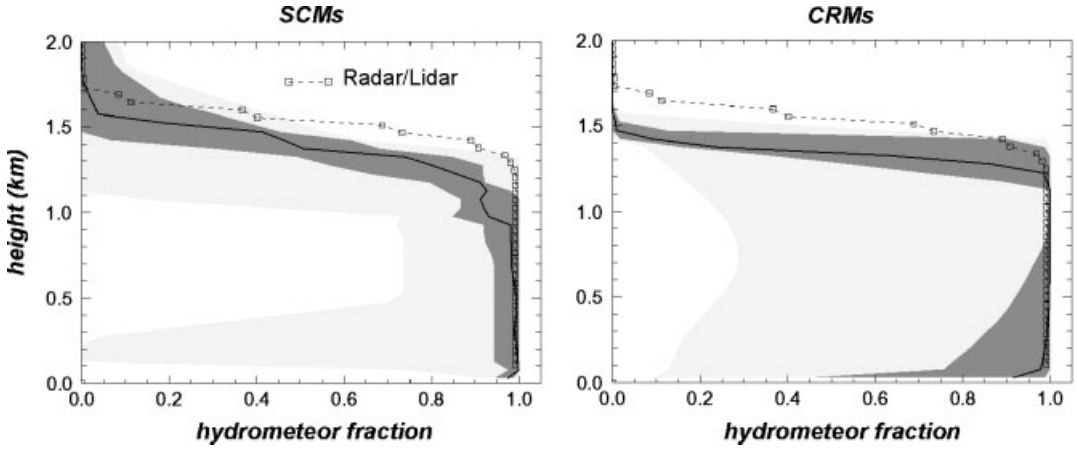

Figure 5. Time-averaged hydrometeor fraction from models and the remote sensors at Barrow (SHUPE-TURNER, dashed line).

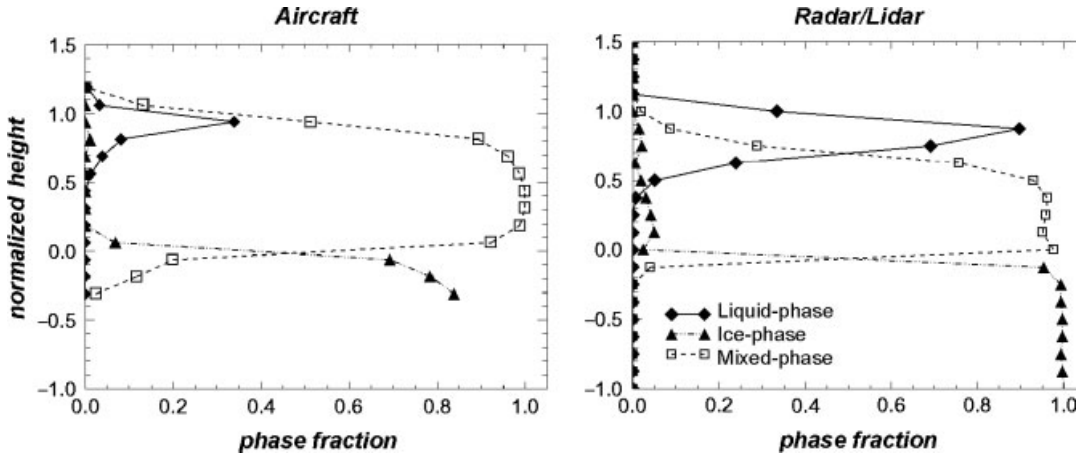

Figure 6. Time-averaged fraction of observations with a given phase as a function of normalized height. Phase categories include liquid-phase only, ice-phase only, and mixed-phase. Normalized height is defined such that 0 is cloud base, 1 is cloud top, and −1 is the surface. The remote sensor retrievals are from SHUPE-TURNER.

ice coexisting in the same volume) with primarily ice-phase precipitation beneath the cloud. Liquid-phase-only condensate is detected on occasion near cloud top.

6.2. Liquid and ice water path

Although models generally produce an overcast precipitating cloud, substantial differences exist in the simulated phase partitioning and mass of cloud condensate. Figure 7 shows a scatter-plot of median liquid water and ice water paths from observations and models. Observations are indicated by letters on the plot: 'A' for aircraft data, 'S' for SHUPE-TURNER retrievals, and 'W' for WANG retrievals. Models are displayed with symbols whose filling indicates whether it is an SCM or CRM and whose shape indicates the class of its microphysical scheme. Medians and interquartile ranges of observational data are presented in Table III and results from individual or sets of models are presented in Table IV.

Because observations do not distinguish cloud from precipitation condensate, vertical integrals of model condensate include precipitation condensate in the reported liquid and ice water paths. For the liquid phase, the contribution of rain to the total water path is always much smaller than the contribution of cloud droplets, whereas for the ice phase, the contribution of snow is often equal to or larger than that of small ice. Graupel makes little or no contribution to the total ice water path in the CRMs. Note that for SCMs, the contribution of rain and snow must be calculated from vertical profiles of the precipitation rate, as mixing ratios of rain and snow are generally not prognostic variables. These precipitation rates were unavailable from some SCMs (ECHAM, GISS, McRAS, McRASI, NCEP and SCRIPPS).

Observations indicate that the cloud system was water-dominated. The retrievals from the ground-based remote sensors at Barrow indicate a liquid water path of about 200 g m^{-2}, whereas the aircraft liquid water path, which is determined from a vertical integral of the profile data, is lower, with values around 120 g m^{-2}. As mentioned previously, some of this difference reflects the east–west gradient in cloud properties; this is further confirmed by the liquid water paths retrieved from the microwave radiometers at Oliktok Point which have values around 100 g m^{-2} (Table III) which is about one-half of the value at Barrow. For the ice phase, both the SHUPE-TURNER and WANG retrievals at Barrow suggest 30 g m^{-2} of ice whereas the aircraft

DOI: 10.1002/qj

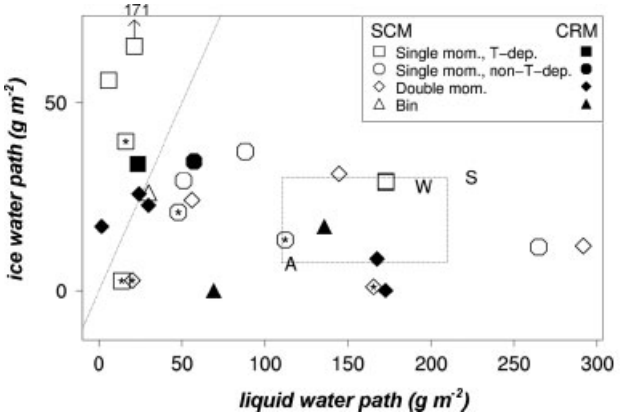

Figure 7. Scatter-plot of the median liquid water path and ice water path from observations (letters) and model simulations (symbols). The aircraft observations are depicted by the letter 'A', whereas the remote sensing retrievals of SHUPE-TURNER and WANG are depicted by the letters 'S' and 'W', respectively. The lightly dashed rectangle indicates the likely range of the regionally averaged liquid and ice water path. The filling or lack thereof in a symbol indicates the model type and the symbol shape indicates the class of model cloud microphysics. See the legend in the plot for the key. As observations do not distinguish between precipitating and non-precipitating condensate, the reported water paths include the contributions from the precipitating species. SCMs for which the precipitation species were unavailable are indicated with a '*' in the centre of the symbol. One model falls outside the plot domain and is depicted with a '↑' attached to its symbol which points to the numerical value of the ordinate. A 1:1 line is plotted for reference.

observations suggest far lower values of around 5 g m^{-2}. In addition to the east–west gradient in cloud properties, some of this difference arises because aircraft totals do not include ice from the lower 60% of sub-cloud air that the aircraft did not sample (Figure 6). Taking into account these factors as well as the uncertainty in the measurements (section 3), a best estimate of the liquid and ice water paths for this period and region would be 160 ± 50 g m^{-2} and 15 g m^{-2} $\pm$ a factor of two (i.e. the ice water path could be between 8 and 30 g m^{-2}), respectively.

Model simulations produce a wide range of results. Although more than three-quarters of models have liquid water paths in excess of ice water paths as observed, two-thirds of models underestimate the observed liquid water path. Median liquid and ice water paths differ little according to model type with values of 56.0 g m^{-2} and 57.3 g m^{-2} for the liquid phase from SCMs and CRMs, respectively, and values of 29.1 g m^{-2} and 17.1 g m^{-2} for the ice phase from SCMs and CRMs (Table IV). Thus, on average, the primary model deficiency is an underestimate of the amount of liquid present in the clouds. Despite this general underestimate, five models (DHARMA, SCAM3, SCAM3-LIU, SCAM3-UW, and UCLA-LARC) have liquid and ice water paths which are consistent with the best estimate of the observations, which is indicated by the lightly dotted rectangle in Figure 7. Two of these models (SCAM3 and SCAM3-UW) achieve good results in part because their specified temperature-dependent partitioning of liquid and ice yields a cloud with 83% liquid at -15°C in rough agreement with observations. However, SCAM3 performs poorly for the simulation presented in Part II where a different ratio of liquid to ice was observed in a cloud with a similar temperature (SCAM3-UW did not participate in Part II). The three other models (DHARMA, SCAM3-LIU, and UCLA-LARC) which are consistent with observations both here and in Part II have more sophisticated cloud microphysics (DHARMA did not participate in Part II). This suggests that it might be beneficial to more closely examine the role of microphysics in producing a good simulation.

Indeed, median liquid and ice water paths appear to approach observed values as the sophistication of the cloud microphysical parametrization increases (Table IV). Specifically, the median liquid water path of the seven models with single moment with T-dependent partitioning is 21.2 g m^{-2}, whereas that of the six models with single moment with independent liquid and ice microphysics is 72.8 g m^{-2}, and that of the ten models with double-moment microphysics is 100 g m^{-2}. The corresponding quantities for ice water path are 33.8, 31.8 and 19.9 g m^{-2}, among these models. However, the three models with bin microphysics do not show improvement over the models with double-moment microphysics.

Despite this general trend, use of a particular class of cloud microphysics does not guarantee a good simulation. For example, half of the ten models with double-moment microphysics have liquid water paths less than 60 g m^{-2}, whereas the other half have liquid water paths in excess of 140 g m^{-2}. The median liquid water path of 100 g m^{-2} is thus a statistical average of a bimodal population of models. Undoubtedly, differences in the representation of boundary layer turbulence or whether it is an SCM or CRM are also responsible for the spread of model results. This is illustrated by examination of two of the three pairs of models that use identical microphysics but differ in the formulation of boundary layer turbulence or whether it is an SCM or CRM. For both of these pairs (ECMWF and ECMWF-DUALM, and ARCSCM and UCLA-LARC, respectively), total condensate water path differs by more than 100 g m^{-2}, demonstrating that simulated cloud properties depend on more than the cloud microphysical scheme employed.

Aerosol–cloud coupling appears to improve the CRM simulations of liquid water path as all CRMs with coupling have liquid water paths greater than CRMs without aerosol–cloud coupling. However, two (NMS-SHIPS and RAMS-CSU) of the four CRMs with aerosol–cloud coupling produce virtually no ice, which in the case of RAMS-CSU is due to precipitation scavenging of all of the initial ice nuclei. Furthermore, SCMs do not display stratification of liquid water paths by aerosol–cloud coupling. From this set of simulations, there does not appear to be a single feature of a model that guarantees a good simulation of the column-integrated amount of liquid and ice; rather, it is likely that a good cloud simulation depends on several high-quality model components functioning well together.

DOI: 10.1002/qj

Table IV. Median condensate water paths from models for simulation hours 4–12.

	Liquid water path (g m^{-2})			Ice water path (g m^{-2})	
	Standard	No ice	High Resolution	Standard	High Resolution
Median model	56.7	208.0	63.1	25.9	26.0
Median SCM	56.0	256.2	64.4	29.1	35.9
Median CRM	57.3	183.6	63.1	17.1	22.8
Median model with single moment with T-dependent partitioning microphysics	21.2	258.6	21.7	33.8	35.9
Median model with single moment with independent liquid and ice microphysics	72.8	263.1	63.1	31.8	28.8
Median model with double moment microphysics	100.0	183.6	195.7	19.9	10.3
Median model with bin microphysics	69.1	–	–	17.0	–
SCMs					
ARCSCM	291.8	358.6	306.0	11.8	9.9
CCCMA	264.9	269.9	336.5	11.5	1.2
ECHAM*	165.5	164.4	239.8	1.0	2.5
ECMWF	5.8	–	–	55.9	–
ECMWF-DUALM	21.2	–	–	171.2	–
GFDL	51.0	278.8	35.0	29.2	27.6
GISS*	47.8	–	–	20.8	–
GISS-LBL	29.8	187.8	–	26.0	–
MCRAS*	13.7	309.1	8.7	2.6	1.2
MCRASI*	20.1	577.8	8.9	2.7	11.3
NCEP*	16.1	60.6	21.7	39.6	56.6
SCAM3	172.9	–	233.6	28.8	35.9
SCAM3-LIU	144.5	–	40.0	31.1	131.5
SCAM3-MG	56.0	–	–	24.0	–
SCAM3-UW	172.9	208.0	126.5	29.1	62.2
SCRIPPS*	112.0	140.4	49.0	13.5	12.3
UWM	88.2	256.2	79.8	37.0	36.0
CRMs					
COAMPS®	24.1	267.3	–	25.7	–
DHARMA	135.7	217.8	–	17.0	–
METO	29.7	77.6	36.7	22.7	24.3
NMS-BULK	1.6	82.0	–	17.1	–
NMS-SHIPS	69.1	65.2	–	0.03	–
RAMS-CSU	172.6	172.8	222.4	0.007	0.014
SAM	23.3	328.5	20.2	33.8	22.8
UCLA-LARC	167.5	194.4	195.7	8.4	10.3
UCLA-LARC-LIN	57.3	–	63.1	34.4	30.0

Results are reported for the standard experiment as well as sensitivity experiments in which ice microphysics are disabled and higher vertical resolution employed. Where available, the rain, snow, graupel water paths are included in the reported total liquid and ice water paths. Asterisks (*) indicate SCMs for which the rain and snow water paths were unavailable. Median ice water paths for sets of models are computed using only models that report snow water paths.

6.3. Liquid and ice water content

Vertical distributions of liquid and ice water content from observations and models on a normalized height coordinate are displayed in Figures 8 and 9. Aircraft measurements indicate that liquid water content increases with height above cloud base which is a characteristic of adiabatic clouds in well-mixed boundary layers. However, the maximum aircraft liquid water content is smaller than the adiabatic value of cloud-top liquid water content which is 0.6 g m^{-3} for a cloud with the aircraft-observed thickness

DOI: 10.1002/qj

of 600 m. The subadiabatic nature of the cloud is consistent with depletion of liquid water by ice precipitation, although cloud-top entrainment may also contribute to the depletion. Because the vertical profile of liquid water content in mixed-phase clouds cannot currently be retrieved, no remote-sensing panel for liquid water content is displayed in Figure 8. Despite this, remote-sensor retrievals also indicate that the cloud at Barrow is less than adiabatic, as the retrieved liquid water path of 195 to 225 g m^{-2} is smaller than the adiabatic liquid water path which is between 235 and 270 g m^{-2} for the observed cloud thicknesses of 700 to 750 m. Although the tendency for greater liquid water content in the upper half of the cloud is not clear in SCM and CRM median values, it is apparent for the highest 25% of models. The low vertical resolution of some SCMs hinders a robust assessment of this point, however. Consistent with the liquid water path, the median model liquid water content is significantly smaller than observed.

The vertical profile of ice water content is generally more uniform than that of liquid water content in both aircraft and remote-sensing observations. Aircraft data indicate median values of 0.01 g m^{-3} which are fairly constant in the cloud and the portion beneath the cloud that the aircraft sampled. The WANG retrievals at Barrow indicate somewhat larger median values in the cloud than in the layer beneath, 0.02 to 0.03 g m^{-3} as compared to 0.01 to 0.02 g m^{-3}. SHUPE-TURNER retrievals are similar. Some of these differences between aircraft and ground-based retrievals are probably due to the east–west gradient in cloud properties, although the differences are within the measurement uncertainty (section 3). A feature of both aircraft and ground-based retrievals is that the distribution of ice water content has a long positive tail with some values in excess of 0.1 g m^{-3}. Model median values are in reasonable agreement with the observations for both SCMs and CRMs. The models' ice water content values are also somewhat greater in the cloud than in the layer beneath. A decrease in ice water content as one approaches the surface would be consistent with sublimation of ice in subsaturated layers near the surface. Also, note that ground-based retrievals of ice water content do not decrease in the layer between normalized height of −0.2 and 0.0 (cloud base), consistent with ice supersaturation in the observed sounding for this layer.

6.4. Surface precipitation

Ice reaching the surface will be observed as surface precipitation. Unfortunately, quantitative estimates of the surface snow rate are highly uncertain. The National Weather Service station in Barrow recorded 0.25 mm d^{-1} for this period. However, for an ice water mixing ratio of 0.01 g m^{-3} at the surface (Figure 9) with an assumed mass-weighted fall speed of 1 m s^{-1}, the precipitation rate would be 0.9 mm d^{-1}. Median surface snow rates of SCMs and CRMs are 0.70 and 0.41 mm d^{-1}, respectively. Although in most models the surface rain rate is zero or very much smaller than the snow rate, there are a few models (CCCMA, ECHAM, RAMS-CSU) in which all surface precipitation is in the form of rain. These models have a high liquid water path but are unable to produce enough ice so that ice precipitation would reach the surface.

6.5. Cloud microphysics

From aircraft observations, median mass-weighted effective radii of liquid and ice are 10 and 25 μm, respectively, and median mass-weighted number concentrations of liquid and ice are 38 cm^{-3} and 2 L^{-1}, respectively. While the ice crystal number concentration of 2 L^{-1} is 12 times larger than the measured ice nuclei concentration of 0.16 L^{-1}, it is in agreement with previous aircraft observations in Arctic clouds with similar temperatures (Jayaweera and Ohtake, 1973; Pinto, 1998; Gultepe *et al.*, 2001). The model median mass-weighted effective radii of liquid and ice are 11 and 67 μm, respectively, and the model median mass-weighted number concentrations of liquid and ice are 55 cm^{-3} and 1.9 L^{-1}, respectively. While these medians are roughly consistent with observed values, general conclusions about the consistency of models with observed values cannot be made due to the very wide range of model results from the roughly 50% of models that submitted the relevant diagnostics.

As an example, the relationship between ice crystal number concentration and liquid water path is examined to ask whether the model-simulated liquid water paths exhibit the inverse relationship with ice crystal number concentration found in prior studies (Harrington *et al.*, 1999; Jiang *et al.*, 2000; Morrison and Pinto, 2006; Prenni *et al.*, 2007). Although ice crystal number concentrations vary over five orders of magnitude among models, the expected inverse relationship is not clearly shown from a scatter-plot of ice crystal number concentration and liquid water path (Figure 10). Contrary to expectations, four models with ice crystal number concentration less than 10 L^{-1} have liquid water paths less than 30 g m^{-2} and one model with a high ice crystal number concentration of 350 L^{-1} has a liquid water path of 165 g m^{-2} consistent with observations. However, in this one model (ECHAM), the high ice crystal number concentration has no direct impact on liquid water path because the ice specific humidity never exceeds a model-imposed threshold of 0.0005 g kg^{-1} required to activate the Bergeron–Findeisen process. Clearly, ice crystal number concentration is only one factor of many influencing the ability of a model to simulate a mixed-phase cloud. Some caution with regard to this figure should be taken as it is not clear that all modellers limited the count of their ice crystal number concentration to particles with diameters greater than 53 μm as was done with the observations (McFarquhar *et al.*, 2007a). Nonetheless, the treatment of model diagnostics is unlikely to explain the very large range of simulated ice crystal number concentrations which most likely results from the widely-varying treatment of ice nucleation among models.

Indeed, differences in ice crystal number concentration between the two models that prognosticate ice nuclei (RAMS-CSU and DHARMA) can likely be explained

DOI: 10.1002/qj

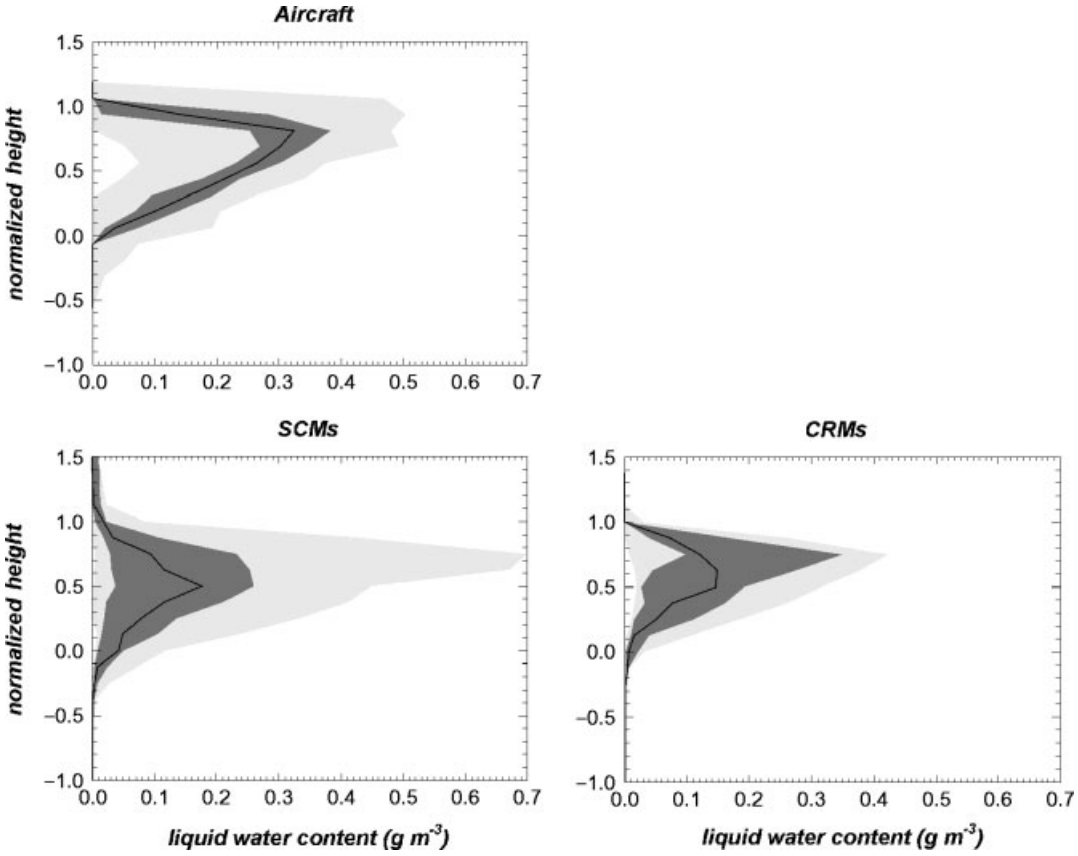

Figure 8. Liquid water content from models and aircraft data as a function of normalized height. Each panel depicts the statistical properties of the profiles including the median value, and the inner and outer 50% of the data as in Figure 4. For the aircraft data, the statistical properties are computed from the high-frequency data. For the models, the statistical properties are computed from the set of model median profile values.

by differences in the modelling of processes that affect ice nuclei. In RAMS-CSU, nearly all initial ice nuclei are consumed by ice precipitation in a few hours, resulting in the lowest ice crystal number concentration of the set (0.003 L^{-1}). A similar result was found in DHARMA using standard microphysical treatments (Fridlind *et al.*, 2007), but the inclusion of a hypothetical process whereby ice nuclei are formed by a tiny fraction of cloud droplet evaporation events leads to larger and sustainable ice number concentrations (4 L^{-1}) as well as a decrease in liquid water path from around 220 to 135 g m^{-2} (the 'evaporation nuclei' treatment shown in Table II of Fridlind *et al.* (2007) was used in this intercomparison).

6.6. Thermodynamic structure

Figure 11 compares time-averaged profiles of total water mixing ratio q_t and ice–liquid water potential temperature θ_{li} from model simulations to the initial condition. The model underestimate of liquid water content is consistent with a reduction of q_t in the upper half of the boundary layer and a vertical gradient of q_t which differs from the initial conditions and is likely unrealistic. Note that a cloud with a liquid water content of two-thirds of the adiabatic value but a water vapour mixing ratio which follows the adiabatic profile of the initial condition (Figure 2) would have a value of q_t at cloud top that is 0.15 g kg^{-1} lower than the value in the sub-cloud layer. Thus observations suggest that this q_t difference should only be 0.15 g kg^{-1}, not the 0.5 g kg^{-1} found in the median model.

In absence of other effects, ice precipitation would stabilize the boundary layer by providing a net heating to the cloud layer and a net cooling to the sub-cloud layer. Although there is some evidence for stabilization in the CRM profiles of θ_{li}, surface fluxes and cloud-top radiative cooling in models with a significant amount of liquid act to keep the boundary layer well-mixed and probably minimize the influence of ice precipitation on vertical stability. Models with greater amounts of cloud liquid water content do show smaller vertical gradients in q_t and θ_{li}.

6.7. Radiation

Figure 12 compares simulations of solar transmission to radiation measurements at Barrow (OBS) and the results of two calculations from a radiative transfer model (STREAMER: Key and Schweiger, 1998) that use the initial condition sounding of temperature and water vapour and along with cloud liquid and ice water paths of 200 and 13 g m^{-2}, respectively. Solar transmission is computed as the average value for the period 1700 UTC 9 October to 0500 UTC 10 October 2004 of the downward short-wave radiative flux at the surface divided by that at the top-of-atmosphere. Solar transmission is plotted

DOI: 10.1002/qj

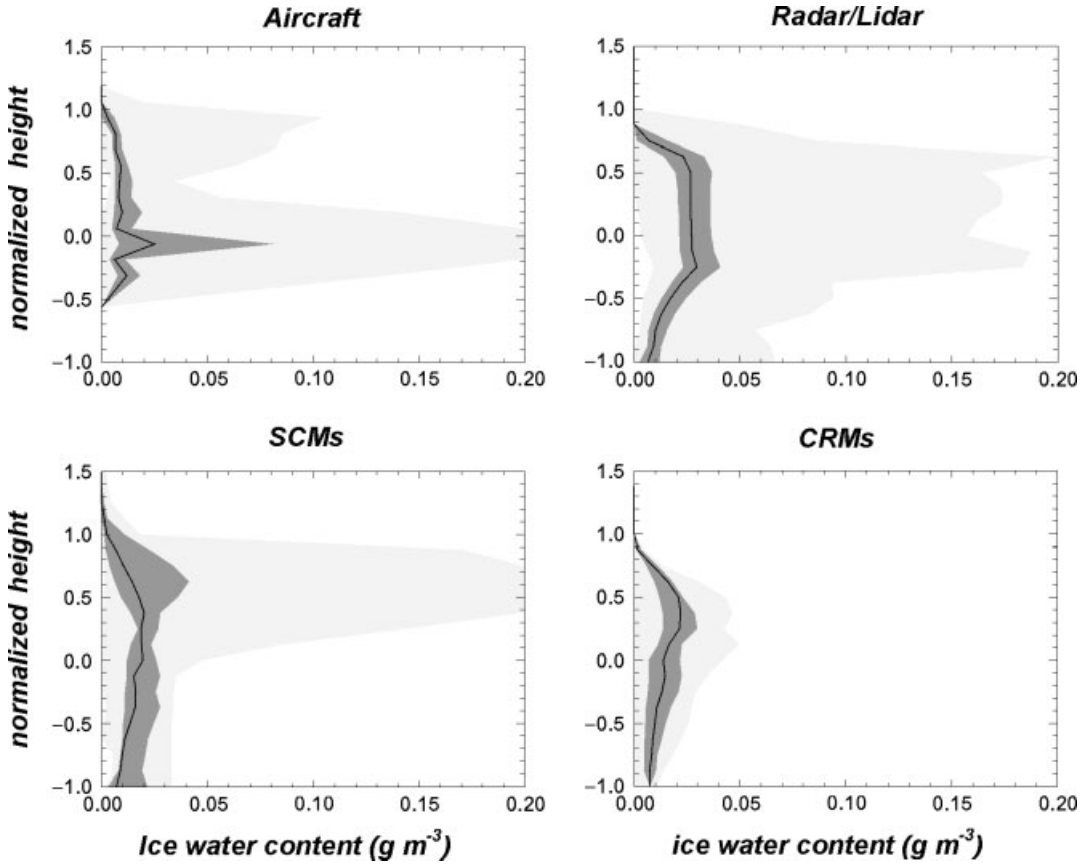

Figure 9. As in Figure 8 but for ice water content. The remote sensing retrievals are from WANG. Note that there are no aircraft data at normalized heights less than −0.6. The SCM plot is constructed by only using the models that report snow water paths.

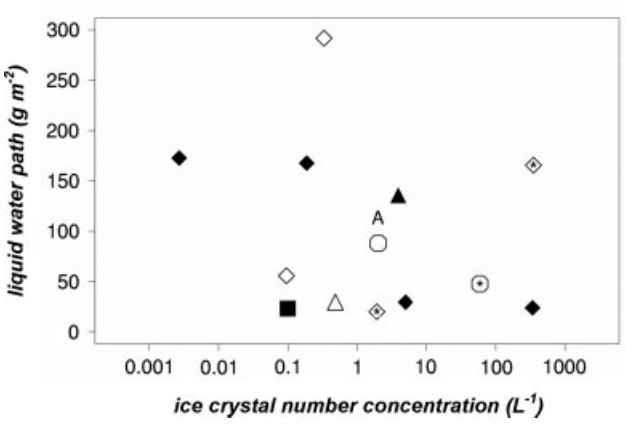

Figure 10. Scatter-plot of the median ice crystal number concentration and liquid water path from aircraft observations (depicted by the letter 'A') and model simulations (symbols). Ice crystal number concentrations are weighted by ice water content and averaged over profiles for the aircraft data and time and height for the models. Symbols are plotted with the same convention as in Figure 7.

together with total condensate water path, although it is not expected that the points will scatter along a single line. As might be expected from the model underestimate of liquid water path, models generally overestimate the solar transmission.

The model overestimate is greater than it appears because simulations used an ocean surface in their radiation calculations. Given that observations were collected over snow-covered land at Barrow, the observed solar transmission is enhanced by multiple reflections between the surface and the cloud. The impact of the different surface albedo can be assessed by comparing STREAMER calculations that use the albedo of an ocean surface (indicated by the letters 'S-O') to those that use the albedo of snow-covered land ('S-L'). Given that STREAMER calculations with a land surface have good agreement with observations, it suggests that models should simulate a solar transmission closer to 0.1 than 0.2.

In the Arctic, the downward component of long-wave radiation at the surface is strongly affected by clouds and is an important quantity that affects the surface temperature of land and sea-ice. Although the surface temperature is fixed in these simulations, it is still important to assess whether the simulated cloud has the correct effect on surface fluxes of radiation. STREAMER calculations with the observed cloud, either over an ocean or land surface, are consistent with the observed value of 280 W m^{-2} (Figure 13). As the downward long-wave radiation is 200 W m^{-2} in clear-sky STREAMER calculations, the long-wave cloud radiative effect is about 80 W m^{-2}. Given that cloud long-wave emissivity is near unity when the condensate water path exceeds about 50 g m^{-2} (Stephens, 1978), it would be expected and is found that models with total condensate water paths greater than this produce long-wave cloud radiative effects consistent with observations (Figure 13).

DOI: 10.1002/qj

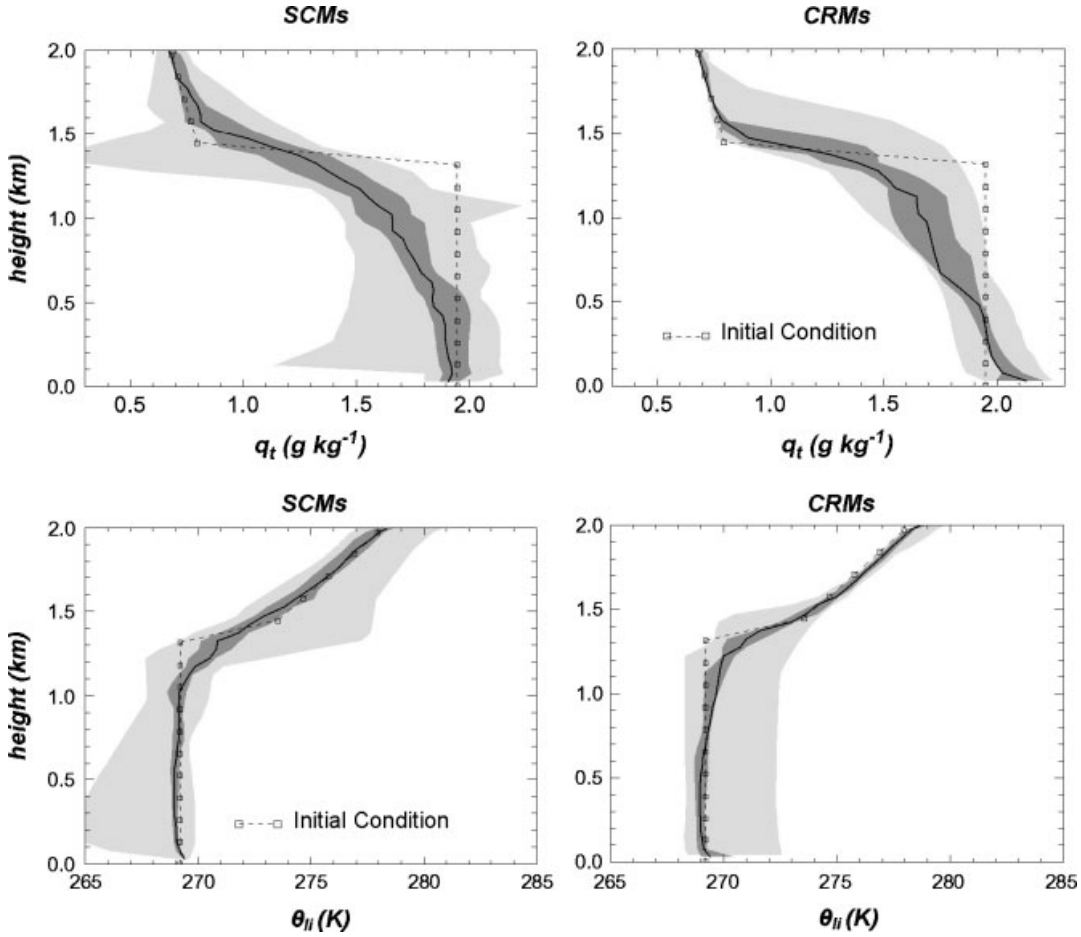

Figure 11. The vertical profiles of total water mixing ratio q_t and ice–liquid water potential temperature θ_{li} from the models. Each panel depicts the statistical properties (median, inner and outer 50%) of the model median profiles as well as the values from the initial condition.

7. Sensitivity studies

7.1. No ice microphysics

Given that numerous modelling studies (Pinto, 1998; Harrington *et al.*, 1999; Jiang *et al.*, 2000; Morrison and Pinto, 2006; Prenni *et al.*, 2007) have demonstrated that the amount of supercooled water in mixed-phase clouds is very sensitive to the representation of ice microphysics in general, and ice crystal number concentration in particular, it is of interest to determine this sensitivity with the present set of models. A sensitivity study was performed in which models were asked to simulate a hypothetical case of a liquid-phase-only cloud. A sensitivity study focused on ice crystal number concentration was not performed because the liquid-phase-only experiment is simple to construct and permits all models to perform a meaningful simulation.

The results demonstrate that there is a large sensitivity of the integrated amount of condensate to the inclusion of ice microphysics (Figure 14). However, this is primarily true in models that have condensate water paths less than 150 g m^{-2} in the control simulation. In these models, the condensate water path in the no-ice-microphysics experiment is greater than that of the control simulation and is often between 200 and 300 g m^{-2}. At least in these models, this suggests that excessive conversion of liquid to ice which easily precipitates is responsible for the underestimate of liquid water path. This is partially confirmed by Figure 15 which shows a general tendency

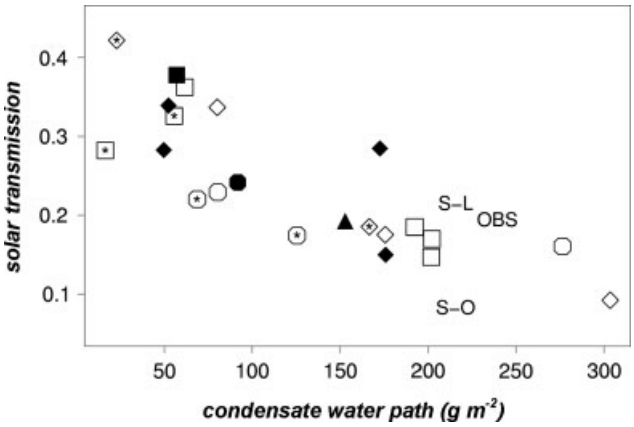

Figure 12. Scatter-plot of solar transmission and total condensate water path. Solar transmission is computed as the average downward component of the broadband solar radiation at the surface divided by the average insolation at the top-of-the-atmosphere. Model results are indicated with symbols with the same convention as in Figure 7. The observations from the radiation measurements and remote sensing retrievals at Barrow are indicated by OBS. The results of STREAMER radiation calculations performed with an ice-free ocean or snow-covered land surface are indicated by S-O and S-L, respectively.

DOI: 10.1002/qj

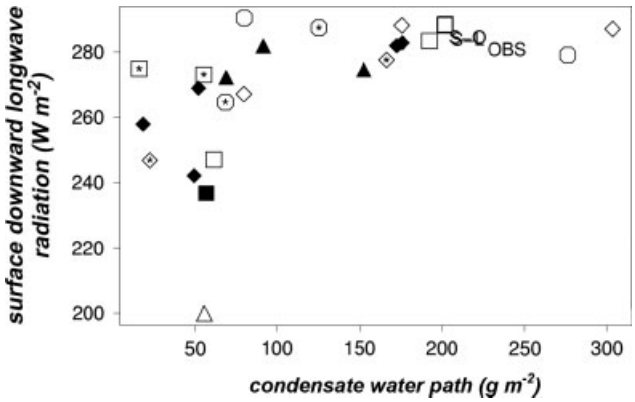

Figure 13. As in Figure 12 but for the downward long-wave radiative flux at the surface.

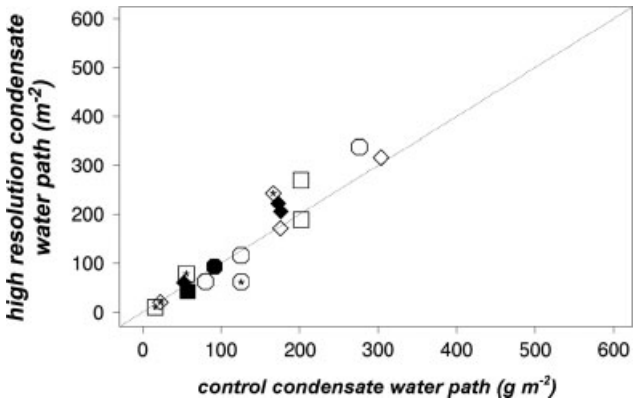

Figure 16. Scatter-plot of the model-simulated total (liquid + ice) condensate water path from a sensitivity study in which models used increased vertical resolution and the control simulations.

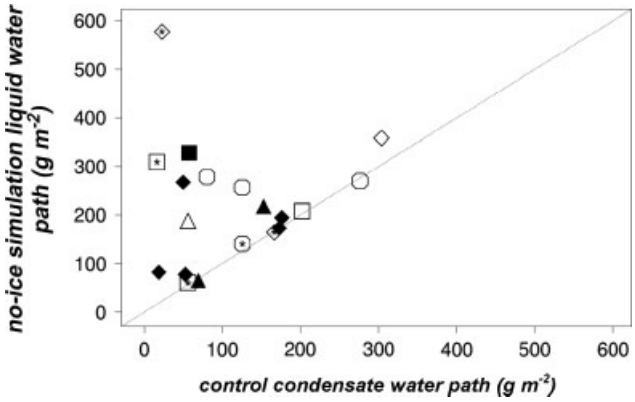

Figure 14. Scatter-plot of the model-simulated liquid water path from a sensitivity study in which ice microphysics was disabled and the total (liquid + ice) condensate water path was from the control simulation. A 1:1 line is shown.

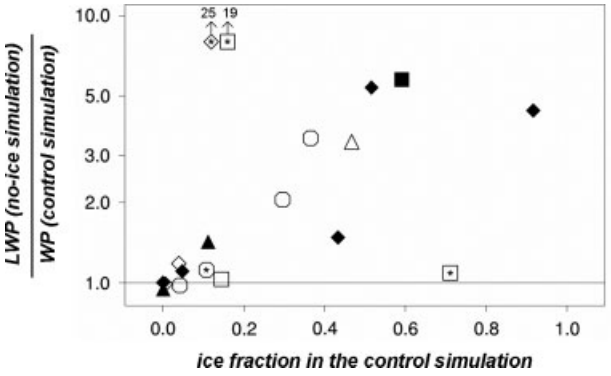

Figure 15. Scatter-plot of the ratio of the total condensate water path in the no-ice sensitivity study to that of the control simulation and the fraction of the total condensate water path in the control simulation that is in the ice-phase. Note that the y-axis is logarithmic and that two models fall outside the plot domain.

for models that have a high fraction of ice in the control experiment to show the greatest relative increase in condensate water path.

The spread in liquid water path and drizzle among SCMs and CRMs is still large in the no-ice-microphysics experiment. SCM liquid water paths vary from 60 to 580 g m^{-2}, while CRM liquid water paths vary from 65 to 330 g m^{-2}. All but four models produce drizzle that reaches the surface at a rate of at least 0.01 mm d^{-1}, with median and maximum precipitation rates of 0.48 mm d^{-1} and 1.6 mm d^{-1}, respectively. This indicates that differences in the representation of processes such as liquid-phase microphysics and boundary-layer turbulence can still lead to significant differences in simulated liquid water path and precipitation. Indeed, recent model intercomparisons of warm-phase stratocumulus also exhibit a wide spread in liquid water path and precipitation (Stevens *et al.*, 2005; Zhu *et al.*, 2005; Wyant *et al.*, 2007).

For models that are sensitive to the inclusion of ice-phase microphysics, the boundary layer tends to be more well-mixed in q_t and θ_{li} relative to the same model in the control experiment, and in sensitive CRMs the boundary layer is slightly deeper. These effects are likely due to greater turbulence near cloud top which is driven by strong cloud-top radiative cooling common to stratocumulus.

7.2. Vertical resolution

Low vertical resolution in atmospheric models in general, and climate models in particular, may lead to non-convergence of simulated cloud properties. Yuan *et al.* (2006) found a significant decrease in liquid and ice water paths as vertical resolution was increased in CCCMA SCM simulations of mixed-phase clouds observed during SHEBA. Modellers were asked to submit a simulation with higher vertical resolution. As vertical resolution in this sensitivity study was not specified, the number of levels in the boundary layer varied from 14 to 146 in the SCMs and from 23 to 53 in the CRMs (Tables I and II). Reassuringly, results indicate a fairly small sensitivity to vertical resolution which is generally much less than the sensitivity to the inclusion of ice microphysics (compare Figure 16 to Figure 14).

8. Summary

An intercomparison of single-column and cloud-resolving model simulations of cold-air outbreak mixed-phase stratocumulus has been presented and evaluated with the

DOI: 10.1002/qj

available ground-based and aircraft observations collected during the ARM Mixed-Phase Arctic Cloud Experiment. While the majority of models reproduce the observed structure of a mixed-phase cloud that produces ice precipitation, the median liquid water path of both SCMs and CRMs is only one-third of the observed value. Thus, there is no evidence that resolving mesoscale and cloud-scale features in the CRMs improves the simulations relative to the SCMs for this case. On the other hand, several models have simulated liquid and ice water paths which are consistent with the observations. Although a general underestimate of liquid water path in Arctic mixed-phase clouds has been found in previous studies (Curry *et al.*, 2000; Inoue *et al.*, 2006; Morrison and Pinto, 2006; Prenni *et al.*, 2007; Sandvik *et al.*, 2007), the present study confirms this result in the context of a highly constrained modelling environment in which identical large-scale advective tendencies and surface fluxes have been applied to a wide range of model types.

There is a trend towards better agreement with observations of liquid and ice water paths as the sophistication of the model microphysics increases from single-moment with temperature-dependent partitioning to single-moment with independent liquid and ice to double-moment. While similar conclusions have been reached in some modelling studies involving Arctic clouds (Girard and Curry, 2001; Morrison and Pinto, 2006), this study involved a wider set of models than these earlier studies. However, also present is a considerable scatter among the models with a given class of microphysics, so it is unclear how much significance to give to this trend. More discussion of this issue will be presented in Part II of this study where a similar trend is also observed.

A sensitivity study in which models simulated a liquid-phase-only cloud indirectly suggests that the interaction of ice microphysics with liquid microphysics is responsible for the significant underestimate of liquid water path present in many models. This calls attention to the widely varying treatment of processes such as ice initiation and the rate at which ice crystals lower the water vapour beneath that necessary to sustain liquid water in the clouds (the Bergeron–Findeisen process). This finding is consistent with previous studies suggesting the importance of ice microphysics in Arctic mixed-phase clouds (Pinto, 1998; Harrington *et al.*, 1999; Jiang *et al.*, 2000; Morrison and Pinto, 2006; Prenni *et al.*, 2007). However, there was also significant scatter among models here in the relationship between liquid water path and ice crystal number concentration which appears contrary to these previous studies. Our results indicate that other factors besides ice crystal number concentration play an important role in producing differences among models. Additionally, it is striking that while models agree relatively well in their simulation of ice water content and path, the simulated ice crystal number concentration varies over five orders of magnitude. A second sensitivity study showed much less dependence of the simulated liquid and ice water paths on the vertical resolution of the model.

Considered as a whole, the results of this study suggest the importance of the treatment of microphysics in general and ice microphysics in particular in the simulation of Arctic mixed-phase clouds. However, microphysics is not the sole factor as other factors are likely to be important. Thus, it is recommended that the GCSS Polar Cloud Working Group conduct additional studies that further constrain simulations. One possible avenue for this work would be to compare different microphysical parametrizations in a framework where dynamical and radiative processes are fixed and non-interactive with simulated cloud microphysics. This may resolve some of the unexplained differences found in the present study and confirm the finding here of overall improvement of simulations with more detailed microphysical parametrizations. In particular, the present case is well-suited for the kinematic framework of Morrison and Grabowski (2007), in which simulations by different microphysical schemes were compared when they were each subjected to the specified flow corresponding to a single large eddy in a stratocumulus-topped boundary layer. It is also recommended that future intercomparison studies constrain the treatment of ice nucleation and ice crystal number concentration.

There may not be a simpler setting for the simulation of mixed-phase clouds. Complications of multilayer cloud systems (Curry *et al.*, 1996) or strong feedbacks between the cloud and the surface temperature and fluxes that happen when mixed-phase clouds are above sea ice (Morrison and Pinto, 2006) have been eliminated in the present case. Despite this simplicity, few model simulations are consistent with observations reflecting the difficulty of simulating these clouds. The intercomparison of model simulations of multilayer clouds observed during M-PACE is presented in Part II of this study.

The relative simplicity of the cloud and its boundary conditions as well as the availability of high-quality observations may make this case-study suitable as a benchmark for mixed-phase clouds. Thin single-layer clouds with high amounts of supercooled liquid water that produce ice precipitation are not limited to the Arctic, but also occur in cold-air outbreaks at lower latitudes (Kristovich *et al.*, 2000) and middle-level cloud systems (Fleishauer *et al.*, 2002; Hogan *et al.*, 2003). It is hoped that this case will continue to be an attractive target for cloud modellers.

Acknowledgements

This work is supported by the Office of Science of the United States (US) Department of Energy under grants DE-AI02-94ER61768 (Del Genio), DE-FG02-02ER63370 (Chen), DE-FG02-02ER63337 (McFarquhar), DE-FG02-03ER63539 (Morrison), DE-FG02-05ER63955 (Cole), DE-FG02-05ER63959 (Park), DE-FG02-05ER64058 (Harrington), DE-FG02-05ER64069 (Wang), DE-AI02-06ER64173 (Ackerman and Fridlind), DE-FG02-06ER64167 (Turner), DE-FG02-06ER64168 (Poellot), DE-AI02-06ER64183

DOI: 10.1002/qj

(Xu), DE-FG02-06ER64187 (de Boer), and DE-FG02-07ER64378 (McFarquhar). A. Ackerman and A. Fridlind are supported by the US National Aeronautics and Space Administration's (NASA) Radiation Sciences Program and the NASA Advanced Supercomputing Division. M. Chen is supported by National Science Foundation (NSF) grant ATM-0415184. J. Cole is supported by the Canadian Foundation for Climate and Atmospheric Sciences. M. Falk and V. Larson are supported by NSF grant ATM-0442605 and subaward G-7424-1 from the Department of Defense Center for Geosciences/Atmospheric Research at Colorado State University via Cooperative Agreement DAAD19-02-2-0005 with the Army Research Laboratory. C. Hoose is supported by the climate programme of the Swiss National Centre of Competence in Research. Y. Luo is supported by the Chinese Academy of Meteorological Sciences and NASA's Cloud Modeling and Analysis Initiative. H. Morrison is supported by NASA grant NNG06GBB1G and by the NSF Science and Technology Center for Multi-Scale Modeling of Atmospheric Processes, managed by Colorado State University under cooperative agreement ATM-0425247. The contribution of S. Klein, R. McCoy, and S. Xie to this work is performed under the auspices of the US Department of Energy by Lawrence Livermore National Laboratory under contract DE-AC52-07NA27344. The Pacific Northwest National Laboratory is operated for the Department of Energy by Battelle Memorial Institute under contract DE-AC06-76RLO-1830. The National Center for Atmospheric Research is sponsored by the National Science Foundation. Gratitude is expressed to A. Beljaars for providing ECMWF analysis data. Comments of R. Pincus and three anonymous reviewers are appreciated.

References

Ackerman AS, Kirkpatrick MP, Stevens DE, Toon OB. 2004. The impact of humidity above stratiform clouds on indirect aerosol climate forcing. *Nature* **432**: 1014–1017.

Ackerman TP, Stokes GM. 2003. The Atmospheric Radiation Measurement program. *Physics Today* **56**: 38–45.

Baumgardner D, Korolev A. 1997. Airspeed corrections for optical array probe sample volumes. *J. Atmos. Oceanic Technol.* **14**: 1224–1229.

Boville BA, Rasch PJ, Hack JJ, McCaa JR. 2006. Representation of clouds and precipitation processes in the Community Atmosphere Model Version 3 (CAM3). *J. Climate* **19**: 2184–2198.

Bretherton CS, Park S. 2009. A new moist turbulence parameterization in the Community Atmosphere Model. *J. Climate*, in press. DOI:10.1175/2008JCL12556.

Chen S and coauthors. 2003. 'COAMPS® version 3 model description: General theory and equations'. Navy Research Laboratory Publication NRL/PU/7500-03-448, Marine Meteorology Division, Monterey, California, 143 pp.

Cober SG, Isaac GA, Korolev AV, Strapp JW. 2001. Assessing cloud-phase conditions. *J. Appl. Meteorol.* **40**: 1967–1983.

Collins WD, Rasch PJ, Boville BA, Hack JJ, McCaa JR, Williamson DL, Briegleb BP, Bitz CM, Lin S-J, Zhang M. 2006. The formulation and atmospheric simulation of the Community Atmosphere Model version 3 (CAM3). *J. Climate* **19**: 2144–2161.

Cotton WR, Pielke Sr RA, Walko RL, Liston GE, Tremback CJ, Jiang H, McAnelly RL, Harrington JY, Nicholls ME, Carrio GG, McFadden JP. 2003. RAMS 2001: Current status and future directions. *Meteorol. Atmos. Phys.* **82**: 5–29.

Curry JA, Rossow WB, Randall DA, Schramm JL. 1996. Overview of Arctic cloud and radiation characteristics. *J. Climate* **9**: 1731–1764.

Curry JA, Pinto JO, Benner T, Tschudi M. 1997. Evolution of the cloudy boundary layer during the autumnal freezing of the Beaufort Sea. *J. Geophys. Res.* **102**: 13851–13860.

Curry JA, Hobbs PV, King MD, Randall DA, Minnis P, Isaac GA, Pinto JO, Uttal T, Bucholtz A, Cripe DG, Gerber H, Fairall CW, Garrett TJ, Hudson J, Intrieri JM, Jakob C, Jensen T, Lawson P, Marcotte D, Nguyen L, Pilewskie P, Rangno A, Rogers DC, Strawbridge KB, Valero FPJ, Williams AG, Wylie D. 2000. FIRE Arctic Clouds Experiment. *Bull. Am. Meteorol. Soc.* **81**: 5–29.

Environmental Modeling Center (EMC). 2003. 'The GFS atmospheric model'. National Center for Environmental Prediction Office Note 442, US Department of Commerce, National Oceanic and Atmospheric Administration, 14 pp. Available online at http://www.emc.ncep.noaa.gov/officenotes/FullTOC.html.

European Centre for Medium Range Weather Forecasts (ECMWF). 2007. 'IFS documentation cycle 31r1. Part IV: Physical processes'. 155 pp. Available online at http://www.ecmwf.int/research/ifsdocs/CY31r1/index.html.

Ferrier BS. 1994. A double-moment multiple-phase four-class bulk ice scheme. Part I: Description. *J. Atmos. Sci.* **51**: 249–280.

Field PR, Hogan RJ, Brown PRA, Illingworth AJ, Choularton TW, Kaye PH, Hirst E, Greenaway R. 2004. Simultaneous radar and aircraft observations of mixed-phase cloud at the 100 m scale. *Q. J. R. Meteorol. Soc.* **130**: 1877–1904.

Flatau PJ, Tripoli GJ, Verlinde J, Cotton WR. 1989. 'The CSU-RAMS cloud microphysics module: General theory and code documentation'. Colorado State University, Department of Atmospheric Science paper No. 451, 88 pp.

Fleishauer RP, Larson VE, Vonder Haar TH. 2002. Observed microphysical structure of midlevel mixed-phase clouds. *J. Atmos. Sci.* **59**: 1779–1804.

Fridlind AM, Ackerman AS, McFarquhar GM, Zhang G, Poellot MR, DeMott PJ, Prenni AJ, Heymsfield AJ. 2007. Ice properties of single-layer stratocumulus during the Mixed-Phase Arctic Cloud Experiment. 2: Model results. *J. Geophys. Res.* **112**: D24202, DOI:10.1029/2007JD008646.

The GFDL Global Atmospheric Model Development Team (GFDL GAMDT). 2004. The new GFDL global atmosphere and land model AM2-LM2: Evaluation with prescribed SST simulations. *J. Climate* **17**: 4641–4673.

Girard E, Curry JA. 2001. Simulation of Arctic low-level clouds observed during the FIRE Arctic Clouds Experiment using a new bulk microphysics scheme. *J. Geophys. Res.* **106**: 15139–15154.

Golaz J-C, Larson VE, Cotton WR. 2002. A PDF-based model for boundary layer clouds. Part I: Method and model description. *J. Atmos. Sci.* **59**: 3540–3551.

Golaz J-C, Wang S, Doyle JD, Schmidt JM. 2005. COAMPS®-LES: Model evaluation and analysis of second- and third-moment vertical velocity budgets. *Boundary-Layer Meteorol.* **116**: 487–517.

Gultepe I, Isaac GA, Cober SG. 2001. Ice crystal number concentration versus temperature for climate studies. *Int. J. Climatol.* **21**: 1281–1302.

Hansen J, Sato M, Nazarenko L, Ruedy R, Lacis A, Koch D, Tegen I, Hall T, Shindell D, Santer B, Stone P, Novakov T, Thomason L, Wang R, Wang Y, Jacob D, Hollandsworth S, Bishop L, Logan J, Thompson A, Stolarski R, Lean J, Willson R, Levitus S, Antonov J, Rayner N, Parker D, Christy J. 2002. Climate forcings in Goddard Institute for Space Studies SI2000 simulations. *J. Geophys. Res.* **107**: 4347, DOI:10.1029/2001JD001143.

Harrington JY, Reisin T, Cotton WR, Kreidenweis SM. 1999. Cloud resolving simulations of Arctic stratus. Part II: Transition-season clouds. *Atmos. Res.* **55**: 45–75.

Hashino T, Tripoli GJ. 2007. The spectral ice habit prediction system (SHIPS). Part I: Model description and simulation of vapor deposition process. *J. Atmos. Sci.* **64**: 2210–2237.

Hobbs PV, Rangno AL. 1998. Microstructures of low and middle-level clouds over the Beaufort Sea. *Q. J. R. Meteorol. Soc.* **124**: 2035–2071.

Hogan RJ, Francis PN, Flentje H, Illingworth AJ, Quante M, Pelon J. 2003. Characteristics of mixed-phase clouds. I: Lidar, radar and aircraft observations from CLARE'98. *Q. J. R. Meteorol. Soc.* **129**: 2089–2116.

Iacobellis SF, Somerville RCJ. 2006. Evaluating parameterizations of the autoconversion process using a single-column model and Atmospheric Radiation Measurement Program measurements. *J. Geophys. Res.* **111**: D02203, DOI:10.1029/2005JD006296.

Illingworth AJ, Hogan RJ, O'Connor EJ, Bouniol D, Brooks ME, Delanoë J, Donovan DP, Eastment JD, Gaussiat N, Goddard JWF,

Haeffelin M, Klein Baltink H, Krasnov OA, Pelon J, Piriou J-M, Protat A, Russchenberg HWJ, Seifert A, Tompkins AM, van Zadelhoff G-J, Vinit F, Willén U, Wilson DR, Wrench CL. 2007. Cloudnet – Continuous evaluation of cloud profiles in seven operational models using ground-based observations. *Bull. Am. Meteorol. Soc.* **88**: 883–898.

Inoue J, Liu J, Pinto JO, Curry JA. 2006. Intercomparison of Arctic regional climate models: Modeling clouds and radiation for SHEBA in May 1998. *J. Climate* **19**: 4167–4178.

Intrieri JM, Shupe MD, Uttal T, McCarty BJ. 2002. An annual cycle of Arctic cloud characteristics observed by radar and lidar at SHEBA. *J. Geophys. Res.* **107**(C10): 8030, DOI:10.1029/2000JC000423.

Jayaweera K, Ohtake T. 1973. Concentration of ice crystals in Arctic stratus clouds. *J. Rech. Atmos.* **7**: 199–207.

Jiang H, Cotton WR, Pinto JO, Curry JA, Weissbluth MJ. 2000. Cloud resolving simulations of mixed-phase Arctic stratus observed during BASE: Sensitivity to concentration of ice crystals and large-scale heat and moisture advection. *J. Atmos. Sci.* **57**: 2105–2117.

Key JR, Schweiger AJ. 1998. Tools for atmospheric radiative transfer: Streamer and FluxNet. *Computers and Geosciences* **24**: 443–451.

Khain AP, Sednev I. 1996. Simulation of precipitation formation in the Eastern Mediterranean coastal zone using a spectral microphysics cloud ensemble model. *Atmos. Res.* **43**: 77–110.

Khairoutdinov MF, Randall DA. 2003. Cloud resolving modeling of the ARM summer 1997 IOP: Model formulation, results, uncertainties, and sensitivities. *J. Atmos. Sci.* **60**: 607–625.

Korolev AV, Field PR. 2008. The effect of dynamics on mixed-phase clouds: Theoretical considerations. *J. Atmos. Sci.* **65**: 66–86.

Korolev AV, Isaac GA. 2003. Phase transformation in mixed-phase clouds. *Q. J. R. Meteorol. Soc.* **129**: 19–38.

Korolev AV, Isaac GA, Cober SG, Strapp JW, Hallett J. 2003. Microphysical characterization of mixed-phase clouds. *Q. J. R. Meteorol. Soc.* **129**: 39–65.

Kristovich DAR, Young GS, Verlinde J, Sousounis PJ, Mourad P, Lenschow D, Rauber RM, Ramamurthy MK, Jewett BF, Beard K, Cutrim E, DeMott PJ, Eloranta EW, Hjelmfelt MR, Kreidenweis SM, Martin J, Moore J, Ochs III HT, Rogers DC, Scala J, Tripoli G, Young J. 2000. The Lake-Induced Convection Experiment and the Snowband Dynamics Project. *Bull. Am. Meteorol. Soc.* **81**: 519–542.

Larson VE, Smith AJ, Falk MJ, Kotenberg KE, Golaz J-C. 2006. What determines altocumulus dissipation time? *J. Geophys. Res.* **111**: D19207, DOI:10.1029/2005JD007002.

Lin Y-L, Farley RD, Orville HD. 1983. Bulk parameterization of the snow field in a cloud model. *J. Appl. Meteorol.* **22**: 1065–1092.

Liu X, Penner JE. 2005. Ice nucleation parameterization for global models. *Meteorol. Zeitschrift* **14**: 499–514.

Liu X, Penner JE, Ghan SJ, Wang M. 2007a. Inclusion of ice microphysics in the NCAR Community Atmospheric Model version 3 (CAM3). *J. Climate* **20**: 4526–4547.

Liu X, Xie S, Ghan SJ. 2007b. Evaluation of a new mixed-phase cloud microphysics parameterization with CAM3 single-column model and M-PACE observations. *Geophys. Res. Lett.* **34**: L23712, DOI:10.1029/2007GL031446.

Lohmann U, Stier P, Hoose C, Ferrachat S, Kloster S, Roeckner E, Zhang J. 2007. Cloud microphysics and aerosol indirect effects in the global climate model ECHAM5-HAM. *Atmos. Chem. Phys.* **7**: 3425–3446.

Luo Y, Xu K-M, Morrison H, McFarquhar GM. 2008a. Arctic mixed-phase clouds simulated by a cloud-resolving model: Comparison with ARM observations and sensitivity to microphysics parameterizations. *J. Atmos. Sci.* **65**: 1285–1303.

Luo Y, Xu K-M, Morrison H, McFarquhar GM, Wang Z, Zhang G. 2008b. Multi-layer Arctic mixed-phase clouds simulated by a cloud-resolving model: Comparison with ARM observations and sensitivity experiments. *J. Geophys. Res.* **113**: D12208, DOI:10.1029/2007JD009563.

McFarquhar GM, Cober SG. 2004. Single-scattering properties of mixed-phase Arctic clouds at solar wavelengths: Impacts on radiative transfer. *J. Climate* **17**: 3799–3813.

McFarquhar GM, Zhang G, Poellot MR, Kok GL, McCoy R, Tooman T, Fridland A, Heymsfield AJ. 2007a. Ice properties of single-layer stratocumulus during the Mixed-Phase Arctic Cloud Experiment. 1: Observations. *J. Geophys. Res.* **112**: D24201, DOI:10.1029/2007JD008633.

McFarquhar GM, Um J, Freer M, Baumgardner D, Kok GL, Mace G. 2007b. Importance of small ice crystals to cirrus properties: Observations from the Tropical Warm Pool International Cloud Experiment (TWP-ICE). *Geophys. Res. Lett.* **34**: L13803, DOI:10.1029/2007GL029865.

Mazin IP. 1986. Relation of clouds phase structure to vertical motion. *Sov. Meteorol. Hydrol.* **N11**: 27–35.

Meyers MP, DeMott PJ, Cotton WR. 1992. New primary ice-nucleation parameterizations in an explicit cloud model. *J. Appl. Meteorol.* **31**: 708–721.

Meyers MP, Walko RL, Harrington JY, Cotton WR. 1997. New RAMS cloud microphysics parameterization. Part II: The two-moment scheme. *Atmos. Res.* **45**: 3–39.

Morrison H, Gettelman A. 2008. A new two-moment bulk stratiform cloud microphysics scheme in the Community Atmosphere Model, version 3 (CAM3). Part I: Description and numerical tests. *J. Climate* **21**: 3642–3659.

Morrison H, Grabowski WW. 2007. Comparison of bulk and bin warm-rain microphysics models using a kinematic framework. *J. Atmos. Sci.* **64**: 2839–2861.

Morrison H, Pinto JO. 2006. Intercomparison of bulk cloud microphysics schemes in mesoscale simulations of springtime Arctic mixed-phase stratiform clouds. *Mon. Weather Rev.* **134**: 1880–1900.

Morrison H, Shupe MD, Curry JA. 2003. Modeling clouds observed at SHEBA using a bulk parameterization implemented into a single-column model. *J. Geophys. Res.* **108**: 4255, DOI:10.1029/2002JD002229.

Morrison H, Curry JA, Khvorostyanov VI. 2005a. A new double-moment microphysics parameterization for application in cloud and climate models. Part I: Description. *J. Atmos. Sci.* **62**: 1665–1677.

Morrison H, Curry JA, Shupe MD, Zuidema P. 2005b. A new double-moment microphysics parameterization for application in cloud and climate models. Part II: Single-column modeling of Arctic clouds. *J. Atmos. Sci.* **62**: 1678–1693.

Morrison H, Pinto JO, Curry JA, McFarquhar GM. 2008. Sensitivity of modeled Arctic mixed-phase stratocumulus to cloud condensation and ice nuclei over regionally varying surface conditions. *J. Geophys. Res.* **113**: D05203, DOI:10.1029/2007JD008729.

Morrison H, McCoy RB, Klein SA, Xie S, Luo Y, Avramov A, Chen M, Cole JNS, Falk M, Foster MJ, Del Genio AD, Harrington JY, Hoose C, Khairoutdinov MF, Larson VE, Liu X, McFarquhar GM, Poellot MR, von Salzen K, Shipway BJ, Shupe MD, Sud YC, Turner DD, Veron DE, Walker GK, Wang Z, Wolf AB, Xu K-M, Yang F, Zhang G. 2009. Intercomparison of model simulations of mixed-phase clouds observed during the ARM Mixed-Phase Arctic Cloud Experiment. II: Multilayer cloud. *Q. J. R. Meteorol. Soc.* **135**: (in press). DOI:10.1002/qj.415.

Neggers RAJ, Köhler M, Beljaars ACM. 2009. A dual mass flux framework for boundary layer convection. Part I: Transport. *J. Atmos. Sci.*, in press. DOI:10.1175/2008JAS2635.1.

Pinto JO. 1998. Autumnal mixed-phase cloudy boundary layers in the Arctic. *J. Atmos. Sci.* **55**: 2016–2038.

Pinto JO, Curry JA, Intrieri JM. 2001. Cloud–aerosol interactions during autumn over Beaufort Sea. *J. Geophys. Res.* **106**: 15077–15097.

Prenni AJ, Harrington JY, Tiernström M, DeMott PJ, Avramov A, Long CN, Kreidenweis SM, Olsson PQ, Verlinde J. 2007. Can ice-nucleating aerosols affect Arctic seasonal climate? *Bull. Am. Meteorol. Soc.* **88**: 541–550.

Randall DA, Krueger S, Bretherton CS, Curry JA, Duynkerke P, Moncrieff M, Ryan B, Starr D, Miller M, Rossow W, Tselioudis G, Wielicki B. 2003. Confronting models with data: The GEWEX Cloud Systems Study. *Bull. Am. Meteorol. Soc.* **84**: 455–469.

Roeckner E, Bäuml G, Bonventura L, Brokopf R, Esch M, Giorgetta M, Hagemann S, Kirchner I, Kornblüh L, Manzini E, Rhodin A, Schlese U, Schulzweida U, Tompkins A. 2003. 'The atmospheric general circulation model ECHAM5. Part I: Model description'. Report 349, Max Planck Institute for Meteorology, Hamburg, Germany. Available from http://www.mpimet.mpg.de.

Rotstayn LD. 1997. A physically based scheme for the treatment of stratiform clouds and precipitation in large-scale models. I: Description and evaluation of the microphysical processes. *Q. J. R. Meteorol. Soc.* **123**: 1227–1282.

Rotstayn LD, Ryan BF, Katzfey JJ. 2000. A scheme for calculation of the liquid fraction in mixed-phase stratiform clouds in large-scale models. *Mon. Weather Rev.* **128**: 1070–1088.

Sandvik A, Biryulina M, Kvamstø NG, Stamnes JJ, Stamnes K. 2007. Observed and simulated microphysical composition of Arctic clouds: Data properties and model validation. *J. Geophys. Res.* **112**: D05205, DOI:10.1029/2006JD007351.

Schmidt GA, Ruedy R, Hansen JE, Aleinov I, Bell N, Bauer M, Bauer S, Cairns B, Canuto V, Cheng Y, Del Genio A, Faluvegi G, Friend AD, Hall TM, Hu Y, Kelley M, Kiang NY, Koch D, Lacis AA, Lerner J, Lo KK, Miller RL, Nazarenko L, Oinas V, Perlwitz J, Perlwitz J, Rind D, Romanou A, Russell GL, Sato M, Shindell DT, Stone PH, Sun S, Tausnev N, Thresher D, Yao M-S. 2006. Present-day atmospheric simulations using GISS Model E: Comparison to *in situ*, satellite, and reanalysis data. *J. Climate* **19**: 153–192.

Shupe MD. 2007. A ground-based multisensor cloud phase classifier. *Geophys. Res. Lett.* **34**: L22809, DOI:10.1029/2007GL031008.

Shupe MD, Intrieri JM. 2004. Cloud radiative forcing of the Arctic surface: The influence of cloud properties, surface albedo, and solar zenith angle. *J. Climate* **17**: 616–628.

Shupe MD, Matrosov SY, Uttal T. 2006. Arctic mixed-phase cloud properties derived from surface-based sensors at SHEBA. *J. Atmos. Sci.* **63**: 697–711.

Shupe MD, Kollias P, Poellot M, Eloranta E. 2008. On deriving vertical air motions from cloud radar Doppler spectra. *J. Atmos. Oceanic Technol.* **25**: 547–557.

Shutts GJ, Gray MEB. 1994. A numerical modelling study of the geostrophic adjustment process following deep convection. *Q. J. R. Meteorol. Soc.* **120**: 1145–1178.

Stephens GL. 1978. Radiation profiles in extended water clouds. II: Parameterization schemes. *J. Atmos. Sci.* **35**: 2123–2132.

Stevens B, Moeng C-H, Ackerman AS, Bretherton CS, Chlond A, de Roode S, Edwards J, Golaz J-C, Jiang H, Khairoutdinov M, Kirkpatrick MP, Lewellen DC, Lock A, Müller F, Stevens DE, Whelan E, Zhu P. 2005. Evaluation of large-eddy simulations via observations of nocturnal marine stratocumulus. *Mon. Weather Rev.* **133**: 1443–1462.

Strapp JW, Albers F, Reuter A, Korolev AV, Maixner U, Rashke E, Vukovic Z. 2001. Laboratory measurements of the response of a PMS OAP-2DC. *J. Atmos. Oceanic Technol.* **18**: 1150–1170.

Stull RB. 1988. *An introduction to boundary layer meteorology*. Kluwer Academic Publishers.

Sud YC, Lee D. 2007. Parameterization of aerosol indirect effect to complement McRAS cloud scheme and its evaluation with the 3-year ARM-SGP analyzed data for single column models. *Atmos. Res.* **86**: 105–125.

Sun Z, Shine KP. 1994. Studies of the radiative properties of ice and mixed-phase clouds. *Q. J. R. Meteorol. Soc.* **120**: 111–137.

Tripoli GJ. 1992. A nonhydrostatic mesoscale model designed to simulate scale interaction. *Mon. Weather Rev.* **120**: 1342–1359.

Turner DD. 2005. Arctic mixed-phase cloud properties from AERI lidar observations: Algorithm and results from SHEBA. *J. Appl. Meteorol.* **44**: 427–444.

Turner DD, Clough SA, Liljegren JC, Clothiaux EE, Cady-Pereira KE, Gaustad KL. 2007. Retrieving liquid water path and precipitable water vapor from Atmospheric Radiation Measurement (ARM) microwave radiometers. *IEEE Trans. Geosci. Remote Sensing* **45**: 3680–3690.

Uttal T, Curry JA, Mcphee MG, Perovich DK, Moritz RE, Maslanik JA, Guest PS, Stern HL, Moore JA, Turenne R, Heiberg A, Serreze MC, Wylie DP, Persson OG Paulson CA, Halle C, Morison JH, Wheeler PA, Makshtas A, Welch H, Shupe MD, Intrieri JM, Stamnes K, Lindsey RW, Pinkel R, Pegau WS, Stanton TP, Grenfeld TC. 2002. Surface heat budget of the Arctic Ocean. *Bull. Am. Meteorol. Soc.* **83**: 255–275.

Verlinde J, Harrington JY, McFarquhar GM, Yannuzzi VT, Avramov A, Greenberg S, Johnson N, Zhang G, Poellot MR, Mather JH, Turner DD, Eloranta EW, Zak BD, Prenni AJ, Daniel JS, Kok GL, Tobin DC, Holz R, Sassen K, Spangenberg D, Minnis P, Tooman TP, Ivey MD, Richardson SJ, Bahrmann CP, Shupe MD, DeMott PJ, Heymsfield AJ, Schofield R. 2007. The Mixed-Phase Arctic Cloud Experiment. *Bull. Am. Meteorol. Soc.* **88**: 205–221.

von Salzen K. 2006. Piecewise log-normal approximation of size distributions for aerosol modelling. *Atmos. Chem. Phys.* **6**: 1351–1372.

Wang Z. 2007. A refined two-channel microwave radiometer liquid water path retrieval for cold regions by using multiple-sensor measurements. *IEEE Geosci. Remote Sensing Lett.* **4**: 591–595.

Wang Z, Sassen K. 2002. Cirrus cloud microphysical property retrieval using lidar and radar measurements. Part II: Midlatitude cirrus microphysical and radiative properties. *J. Atmos. Sci.* **59**: 2291–2302.

Wyant MC, Bretherton CS, Chlond A, Griffin BM, Kitagawa H, Lappen C-L, Larson VE, Lock A, Park S, de Roode SR, Uchida J, Zhao M, Ackerman AS. 2007. A single-column model intercomparison of a heavily drizzling stratocumulus-topped boundary layer. *J. Geophys. Res.* **112**: D24204, DOI:10.1029/2007JD008536.

Xie S, Xu K-M, Cederwall RT, Bechtold P, Del Genio AD, Klein SA, Cripe DG, Ghan SJ, Gregory D, Iacobellis SF, Krueger SK, Lohmann U, Petch JC, Randall DA, Rotstayn LD, Somerville RCJ, Sud YC, von Salzen K, Walker GK, Wolf A, Yio JJ, Zhang GJ, Zhang M. 2002. Intercomparison and evaluation of cumulus parametrizations under summertime midlatitude continental conditions. *Q. J. R. Meteorol. Soc.* **128**: 1095–1135.

Xie S, Klein SA, Yio JJ, Beljaars ACM, Long CN, Zhang M. 2006. An assessment of ECMWF analyses and model forecasts over the North Slope of Alaska using observations from the ARM Mixed-Phase Arctic Cloud Experiment. *J. Geophys. Res.* **111**: D05107, DOI:10.1029/2005JD006509.

Xie S, Boyle J, Klein SA, Liu X, Ghan S. 2008. Simulations of Arctic mixed-phase clouds in forecasts with CAM3 and AM2 for M-PACE. *J. Geophys. Res.* **113**: D04211, DOI:10.1029/2007JD009225.

Xu K-M, Krueger SK. 1991. Evaluation of cloudiness parameterizations using a cumulus ensemble model. *Mon. Weather Rev.* **119**: 342–367.

Yuan J, Fu Q, McFarlane N. 2006. Tests and improvements of GCM cloud parameterizations using the CCCMA SCM with the SHEBA data set. *Atmos. Res.* **82**: 222–238.

Zhao QY, Carr FH. 1997. A prognostic cloud scheme for operational NWP models. *Mon. Weather Rev.* **125**: 1931–1953.

Zhu P, Bretherton CS, Köhler M, Cheng A, Chlond A, Geng Q, Austin P, Golaz J-C, Lenderink G, Lock A, Stevens B. 2005. Intercomparison and interpretation of single-column model simulations of a nocturnal stratocumulus-topped marine boundary layer. *Mon. Weather Rev.* **133**: 2741–2758.

Zuidema P, Baker B, Han Y, Intrieri JM, Key JR, Lawson P, Matrosov S, Shupe MD, Stone R, Uttal T. 2005. An Arctic springtime mixed-phase cloudy boundary layer observed during SHEBA. *J. Atmos. Sci.* **62**: 160–176.